

Flow Separation Control on a NACA 0015 Airfoil using Co-Flow Jet (CFJ) Flow

By

Md. Amzad Hossain



A Project submitted in partial fulfillment of the requirements for the degree of Master of
Science in Engineering in the Department of Mechanical Engineering



Khulna University of Engineering & Technology
Khulna 9203, Bangladesh
December, 2013

Declaration

This is to certify that the project work entitled "*Flow Separation Control on a NACA 0015 Airfoil using Co-Flow Jet (CFJ) Flow*" has been carried out by *Md. Amzad Hossain* in the Department of *Mechanical Engineering*, Khulna University of Engineering & Technology, Khulna, Bangladesh. The above project work or any part of this work has not been submitted anywhere for the award of any degree or diploma.

Md. Mashud
15-12-13

Signature of Supervisor
Name: Dr.Mohammad Mashud
Designation: Professor

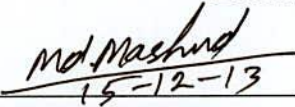
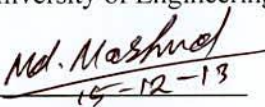
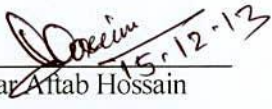

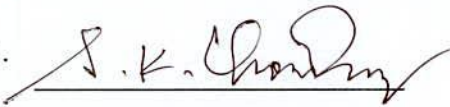
1 (A)
15-12-13

Signature of Candidate
Name: Md. Amzad Hossain
Roll No.: 1105551

Approval

This is to certify that the project work submitted by *Md. Amzad Hossain* entitled "*Flow Separation Control on a NACA 0015 Airfoil using Co-Flow Jet (CFJ) Flow*" has been approved by the board of examiners for the partial fulfillment of the requirements for the degree of *Master of Engineering* in the Department of *Mechanical Engineering*, Khulna University of Engineering & Technology, Khulna, Bangladesh in December' 2013.

BOARD OF EXAMINERS

1. 
15-12-13
Chairman
(Supervisor)
Dr. Mohammad Mashud
Professor, Department of Mechanical Engineering
Khulna University of Engineering & Technology
2. 
15-12-13
Member
Head of the Department
Department of Mechanical Engineering
Khulna University of Engineering & Technology
3. 
15.12.13
Member
Dr. Khandkar Aftab Hossain
Professor, Department of Mechanical Engineering
Khulna University of Engineering & Technology
4. 
15.12.13
Member
Dr. Mohammad Ariful Islam
Professor, Department of Mechanical Engineering
Khulna University of Engineering & Technology
5. 
Member
(External)
Dr. Sirajul Karim Choudhury
Professor, Department of Mechanical Engineering
Rajshahi University of Engineering & Technology, Rajshahi

Acknowledgements

At first it is the author's immense pleasure to express his praise and gratitude to the Merciful Allah, who makes him capable to successfully complete this study. The author is profoundly indebted to his supervisor Dr. Mohammad Mashud, Professor, Department of Mechanical Engineering, Khulna University of Engineering & Technology, Bangladesh, for his proper guidance, inspiration, suggestion and all kinds of supports in performing and completing the dissertation works in time. The author also wishes to express his heart-felt gratitude to his advisor who tolerated his shortcomings; showed patience in author's all kind of activities relevant to research works, remove intricacy in research works and made him confidence enough in the research field. The author would like to express his sincere appreciation and gratitude to Head of the Department, Department of Mechanical Engineering, Khulna University of Engineering & Technology, Bangladesh for his cooperation to create sufficient laboratory facilities for carrying out part of the research works in this University and potential encouragement from the beginning.

Warmest and sincere thanks are extended to Md.Assaduzzaman, former student of this department for his help to setup the airfoil in wind tunnel.

The author would like to express his sincere gratitude and thanks to the Vice Chancellor of Khulna University of Engineering & Technology for financial support during research period. Also, the patience, understanding, moral support and cooperation of the author's parents and family are deeply acknowledged. May Allah bless and reward all of them.

Author

Abstract

This thesis describes the effort to experimentally verify the high performance characteristics of the co-flow jet (CFJ) airfoil. The CFJ utilizes tangentially injected air at the leading edge and tangentially removed air at the trailing edge to increase lift and stall margin and also decrease drag. The mass flow rates of the injection and suction are equal, so there is a zero net mass flow rate. The existing ME subsonic Aerolab wind tunnel with a one-meter by one-meter test section was modified to accommodate the injection and suction needed for the CFJ airfoils. The compressor and vacuum systems were reconfigured so the mass flow rate of air could be measured and controlled. The sting balance used to hold the airfoil in the test section and gather lift and drag information was also modified from a previous design. One modified airfoil CFJ NACA 0015 and one Basic Airfoil NACA 0015 were tested at KUET. The injection slot and suction slot of Modified airfoil CFJ NACA 0015 had the same slot height which is 0.195 m or 0.65% of chord length. The smaller injection slot size performed superior for increased lift and stall margin, whereas the larger injection slot size performed superior for decreased drag. This type of modified airfoil improved the lift percentage to 82.5% (stall AOA) and a decrease in drag to 16.7% at $AoA=25$ deg and $C_{\mu}=0.07$ when compared to the baseline airfoil. When the mass flow rate was run at high levels, negative drag (i.e., thrust) was measured for both airfoils.

Contents

	PAGE
Title Page	i
Declaration	ii
Certificate of Research	iii
Acknowledgement	iv
Abstract	v
Contents	vi
List of Tables	viii
List of Figures	ix-x
CHAPTER ONE INTRODUCTION AND BACKGROUND	1-5
1.1 Introduction	1-2
1.2 Background	2-3
1.3 Objectives	4
1.4 Applications	4-5
CHAPTER TWO Literature Review	6-13
2.1.1 Active flow separation control techniques	7-10
2.1.2 Passive flow separation control techniques	10-12
2.1.3 Co-flow jet airfoil concept	13
CHAPTER THREE Model Design AND Model Construction	24-17
3.1 Model Design	14-17
3.2 Model Construction	17-19
CHAPTER FOUR APPARATUS MODIFICATIONS AND ASSEMBLY	20-33
4.1 Co-Flow Jet Airfoil Description	20-21
4.2 Wind Tunnel Modifications	21-24

4.3 Mass Flow Rate Controls	25-26
4.4 Balance Modifications	26-27
4.5 Calibration of Airfoil	27
4.6 Instrumentation and Measurements	28-29
4.7 Uncertainty Analysis	29-33
CHAPTER FIVE PROCEDURE	34
CHAPTER SIX DISCUSSION OF RESULTS	35-42
6.1 Different Tests Conducted	35-39
6.2 Improved Lift, Drag and Stall	39-41
6.3 Flow Visualization effect	42
CHAPTER SEVEN CONCLUSION AND RECOMMENDATION	43
REFERENCES	45-46
APPENDIX A DETAILED CALIBRATION PROCEDURE	47
APPENDIX B LIST OF INSTRUMENTATION AND EQUIPMENT	48
APPENDIX C DETAILED AIRFOIL ASSEMBLY PROCEDURE	49
APPENDIX D DETAILED WINDTUNNEL ASSEMBLY PROCEDURE	50



LIST OF TABLES

Table No.	Description	Page
4.1	Orifice plate 1494 coefficients	26
4.2	List of the Uncertainties of the measured value	30
4.3	Uncertainty in orifice plate calculation	31

List of Figures

Figure No	Description	page
Fig. 2.1.1.1:	Components of an electrodynamic synthetic jet. Figure from Cattafesta [2011].	08
Fig. 2.1.1.2:	PIV visualization of flow separation postponement on a wind turbine blade by applying synthetic jets at $\alpha = 16^\circ$ and $Re = 1.6 * 10^5$. Figure from Maldonado et al. [2010].	08
Fig. 2.1.1.3:	Working principle of boundary layer suction. Figure from Boermans [2008]	08
Fig. 2.1.1.4:	Schematization of a piezoelectric flap. Figure from Veldhuis and van der Jagt [2010].	09
Fig. 2.1.1.5:	Schematization of a DBD plasma actuator. Figure from LeBeau [2007].	10
Fig. 2.1.2.1:	Vortex generators displayed in different setups. Figures from von Stillfried et al. [2010].	11
Fig. 2.1.2.2:	Lift-enhancing tabs as used by Lee et al. [2005].	12
Fig. 2.1.3.1:	Baseline airfoil and the air-foil with co-flow jet slot.	13
Fig.3.1.1:	Airfoil nomenclature.	15
Fig.3.2.1:	NACA 0015 airfoil profile	18
Fig. 3.2.2:	CFJ 0015-065-065 airfoil.	19
Figure 4.1:	2-D and 3-D cross section of CFJ airfoil	21
Figure 4.2:	Unmodified Aerolab wind tunnel	22
Figure 4.3:	Modified Aerolab wind tunnel	22
Figure 4.4:	Hose/clamp attachment to cylinder and balance mechanism. Airfoil is attached in horizontal position inside tunnel.	23
Figure 4.5:	Connection between the balance cylinder and the airfoil	24
Figure 4.6:	Connection between the suction manifold and the airfoil	24
Figure 4.7:	Plexiglas box and suction manifold with airfoil located to the left and external suction connection to the right	24
Figure 6.1:	Injection Velocity vs. AoA at different mass flow rate.	35
Figure 6.2 :	C_μ vs. AOA at Different Mass flow Rate	36
Figure 6.3:	$-C_p$ vs. x/c at AoA= 05 deg.	37
Figure 6.4:	$-C_p$ vs. x/c at AoA= 15 deg.	38
Figure 6.5:	$-C_p$ vs. x/c at AoA= 25 deg.	39

Figure 6.6: Lift coefficient verse angle of attack for CFJ0015-065-065 at $C_{\mu}=0.07$ and $Re=1.89 \times 10^5$	40
Figure 6.7: Drag Coefficient vs. AOA for CFJ0015-065-065 at $C_{\mu}=0.07$ and $Re=1.89 \times 10^5$	41
Figure 6.8: C_l vs. C_d curve at $C_{\mu}=0.07$ and $Re=1.89 \times 10^5$	41
Figure 6.9: Smoke Flow Visualization for (a) Baseline and (b) CFJ ($C_{\mu}=0.14$) at $AoA=25^\circ$	42

CHAPTER ONE

INTRODUCTION AND BACKGROUND

1.1 INTRODUCTION

The objective of the wind tunnel experiments described in this thesis is to verify the high performance capabilities of the co-flow jet (CFJ) airfoil. This new flow control technique was suggested by Zha and Paxton [1]. The CFJ uses circulation control to achieve this high performance. More specifically, the CFJ uses leading edge blowing and trailing edge suction. This thesis also presents the effort it took to set up and test the CFJ airfoil. Many modifications were made to existing system to implement the injection and suction needs of the CFJ airfoil.

Flow control offers many benefits to aircraft for both commercial and military uses. The primary advantage of these control techniques is the enhanced lift and suppressed separation. Results of these benefits are shorter take-off and landing distances, increased manoeuvrability, increased payloads, reduced fuel consumption and reduced weight.

There are a number of flow control techniques that are being used today. These include rotating cylinders at the leading and trailing edge [2], blowing at the leading edge [3, 4], blowing at the trailing edge [5-7], pulsating jets [8-10] and multi-element airfoils [11, 12].

The CFJ has advantages over the flow control methods mentioned by requiring no moving parts, not requiring a feedback control system and having a net mass flow rate of zero. Moving parts add weight to the aircraft. Feedback control systems add complexity and could also add weight to the aircraft. Blowing air has a direct and adverse effect on the propulsion system if it is taken from the compressor stage of the engine or adds weight to the aircraft if a compressor system is added. The mentioned control systems are limited by one or more of these constraints.

Another advantage of the CFJ is that it can be implemented on any airfoil shape. It can be used on a thick subsonic airfoil as well as a thin supersonic airfoil. Some of the other flow control techniques need thick leading or trailing edges, which drastically increase the drag force during cruise and limit the number of airfoils to which the technique is applicable.

The CFJ has proven to be effective at increasing lift and stall margin while decreasing drag at the same time [13]. This is accomplished with little penalty to the propulsion system by having a net mass flow rate of zero as mentioned earlier. The mass of air that is injected at the leading edge is equal to the mass of air that is removed at the trailing edge. The pulsed jet or synthetic jet, another zero mass flow rate technique, increases $C_{L\ max}$ by about 35% and has little effect on the Stall angle for a jet momentum Coefficient of 0.022 [9]; whereas the CFJ increases $C_{L\ max}$ by 82.5% and decreases Drag by 16.5% at Stall AOA and $C_{\mu} = 0.07$ when compared to the baseline airfoil.

1.2 Background:

Flow control is playing a more and more important role to improve aircraft aerodynamic Performance [1][2]. To enhance lift and suppress separation, various flow control techniques have been used including rotating cylinder at leading and trailing edge[3][4][2], circulation control using tangential blowing at leading edge and trailing edge[5][6] [7][8][9][10], multi-element airfoils[11][12], pulsed jet separation control[13][14][15], etc. The different flow control methods have their different features. For example, the rotating cylinder and circulation control are generally most effective when the leading edge or trailing edges are thick. The multi-element airfoil can generate very high lift, but generally comes with large drag penalty.

This thesis paper applies the new flow control technique of the co-flow jet cascade to high lift airfoil since both experience severe adverse pressure gradient at high loading. Unlike the conventional circulation control airfoils, for which the jets are mostly implemented at leading and trailing edge, the co-flow jet (CFJ) airfoil is implemented on the majority area of the suction surface of the airfoil. The co-flow jet airfoil is to open a long slot on the airfoil suction surface from near leading edge to near trailing edge. A high energy jet is then injected

near the leading edge tangentially and the same amount of mass flow is sucked away near the trailing edge. The turbulent shear layer between the main flow and the jet causes a strong turbulence diffusion and mixing, which enhance the lateral transport of energy and allow the main flow to overcome the severe adverse pressure gradient and stay attached at high angle of attack (AOA). At a certain AOA, the airfoils always achieve a significantly higher lift due to the augmented circulation. The operating range of AOA, hence the stall margin, is also significantly increased. The co-flow jet airfoil does not rely on the Coanda effect at the leading or trailing edge, and hence the thick leading or trailing edges are not required. The technique can apply to any type of airfoils including the modern high speed thin airfoil, and can be combined with other flow control techniques.

When a flow control technique for airfoil is developed, we have to consider the overall airframe-propulsion system to make sure that the benefit outweighs the penalty. For the proposed co-flow jet airfoil, since the jet blows and sucks the same amount of the mass flow, the jet hence can be recalculated to reduce the energy expenditure of the overall airframe-propulsion system compared to the blowing only method such as the circulation control. The jet blowing flow is usually from the engine. For the blowing only method, the high energy jet is dumped out and that is a penalty to the engine efficiency since the engine needs to energize the flow from the low energy free stream. The jet has higher energy state than the free stream flow even near the trailing edge. Hence less work needs to be done to energize the flow for blowing and the overall cycle efficiency can be higher. In addition to recirculating the jet flow, another energy saving of this flow control method is that it is desirable to blow the jet near leading edge where the pressure is low and to suck the jet near the trailing edge where the pressure is high.

Different from the conventional circulation control (CC) airfoil which may be most suitable for taking off and landing, the CFJ airfoil can be used for the whole flying mission from taking off, cruise, maneuver, to landing. No moving parts are needed and make it easy to be implemented and weight less. The CFJ airfoil does not require large leading edge (LE) or trailing edge (TE) and hence has small form drag as the regular modern airfoil.

A CC airfoil relies on local favourable pressure gradient on a curved surface to make the flow attached, the Coanda effect. Such favourable pressure gradient exists at the airfoil leading edge due to the suction and at the end of the trailing edge due to the low base pressure when

the trailing edge is blunt. To make the CC airfoil effective, the blunt TE is hence needed, which is also the reason to create large drag at small AOA such as at cruise. At large AOA, because the main flow cannot resist the large adverse pressure gradient, the local TE favourable pressure gradient cannot be achieved and hence the Coanda effect is difficult to maintain. If only TE blowing is used, the CC airfoil will usually stall at smaller AOA than the non-CC airfoil with sharp TE. The CFJ airfoil significantly increases the AOA range and hence increases the safety margin of the aircraft. Above limitations of the CC airfoil may be part of the reasons that the CC airfoil has not been used for realistic aircraft so far.

For the CFJ airfoil, when the AOA is not large such as at cruising point, the pressure gradient may not be very severe. When the co-flow jet is used to enhance the lift, the main flow around the airfoil is energized and the wake is filled to have a shallow defect shape or even protruding shape. This will reduce the drag or generate thrust (negative drag) for the airfoil. Obviously, there may be an optimum jet control to be most energy efficient. For example, it may be the optimum to achieve zero drag instead of the negative drags (thrust) because the airfoil may not be an efficient propulsion system. The filled wake will generate low noise level since there is no wake mixing. The noise level could be lower than the CC airfoil which has little wake filling effect. The enhanced lift can reduce the wing span for easy storage and reduced wet area and skin friction. The enhanced lift can also significantly shorten the taking off and landing distance. Basically, we can effectively trade the thrust to lift through CFJ at short landing and taking off without using vectored device. The special mechanism of the CFJ airfoil makes it work able for the full flying envelop.

1.3 Objectives:

The aim of the project is to experimentally investigate the performance of airfoil characteristics by co-flow jet flow control method in order to reduce the Drag coefficient, increase the Lift coefficient, and control the Flow separation over airfoil geometry.

1.4 Applications:

The flow separation is mostly an undesirable phenomenon and an effective flow separation control system can be used for enhancing lift, dramatically reduce drag and can achieve very high C_l/C_d (infinity when $C_D = 0$) at low AOA (cruise), and very high lift and drag at high AOA (takeoff and landing); Significantly increase AOA operating range and stall margin;

have small penalty to the propulsion system; can be applied to any airfoil, thick or thin; can be used for whole flying mission instead of only take-off and landing; can be used for low and high speed aircraft; easy implementation with no moving parts.

The above advantages of flow separation control may derive the following superior aircraft performances: 1) Extremely short distance for take-off and landing; 2) Supersonic aircraft to have small wing size matching cruise need, but also have high subsonic performance (e.g. high lift low drag at $M < 1$); 3) High maneuverability, high safety and fast acceleration military aircraft; 4) Very economic fuel consumption; 5) Small wing span for easy storage, light weight and reduced skin friction and form drag; 6) Low noise due to no high lift flap system and weakened wake mixing.

CHAPTER TWO

Literature Review

Flow control is one of the most important research areas in the fluid mechanics that has been investigated by many researchers for more than 50 years. One of the important targets of the flow control is to control flow separation with respect to overall drag reduction. Separation delay and resulting separation zone shortening are of great interest in a number of industrial branches, e.g. turbo machinery, car and aircraft aerodynamics, etc. The separation of the boundary layer is associated with large energy losses and in most applications adversely affects the aerodynamic loads in the form of lift loss and drag increase. Therefore, there is a strong tendency to delay the occurrence of flow separation. Reduction of drag on the wing of an air plane can reduce fuel consumption and saves more energy. Turbulent boundary layer has more surface friction than laminar boundary layer, thus by keeping the flow laminar over the wing skin friction reduces. There are various approaches to control flow separation over an airfoil. These approaches can be divided into two types of flow separation control techniques: active flow separation control and passive flow separation control. Active flow separation control techniques are based on putting energy into the flow, while passive control techniques do not induce energy in the system. In practice, active flow separation control can lead to higher lift performance improvements compared to passive techniques, often at the cost of increased complexity of the system. Both flow control techniques are based on either directly increasing the momentum in the boundary layer or by creating vortices transporting higher momentum free stream flow to within the boundary layer. Increasing the momentum of a boundary layer will generally increase the ability to overcome the adverse pressure gradient.

2.1.1 Active flow separation control techniques:

The active flow control techniques can be classified into the following solutions: fluidic, moving object/surface, plasma and others. This section will briefly describe each of these control techniques [16].



Fluidic actuators

Fluidic actuators use fluid injection or suction to obtain a certain amount of control on the flow. Although many subclasses exist, the two most commonly used fluidic actuators are synthetic jets and boundary layer suction/blowing.

Figure 2.1.1.1 shows a schematic of an electrodynamic synthetic jet configuration. Synthetic jets are based on alternately ingesting and expelling fluid into the flow to create vortices and a higher momentum boundary layer. For the actuator shown in figure 2.1.1.1 this is done by a diaphragm, which will oscillate under influence of electrodynamic transduction. The magnet generates a magnetic field with a magnetic flux density, which under the influence of an alternating current (AC-current) in the wound coils, results in an alternating force induced on the coils. This causes the diaphragm to oscillate, which results in fluid flowing in and out the cavity through an orifice or slot leading to vortices in the boundary layer. Maldonado et al. [2010] performed PIV measurements on wind turbine blades equipped with synthetic jets at high angle of attack. Significant improvements in $C_{L,max}$ were found in the order of 12% at a delayed stall angle of 2° compared to the baseline configuration. The delay in flow separation on the turbine blade is illustrated in figure 2.1.1.2.

Boundary layer suction/blowing is another way to increase the momentum in the boundary layer. With boundary layer suction this is done by removing the low momentum flow in the vicinity of the wall, where usually the fluid is expelled at another location. Boundary layer blowing directly increases the momentum of the boundary layer and can even be done oscillatory to add vortices to the flow as well. Figure 2.1.1.3 graphically explains the working principle of boundary layer suction.

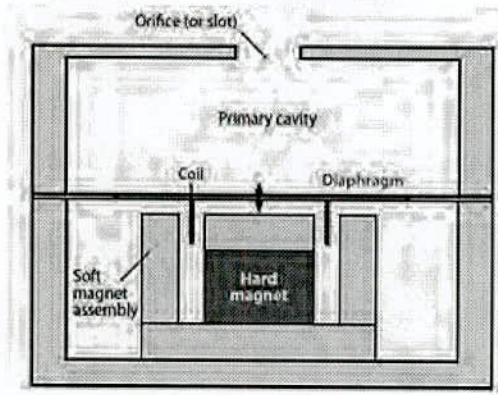


Fig. 2.1.1.1: Components of an electrodynamic synthetic jet. Figure from Cattafesta [2011].

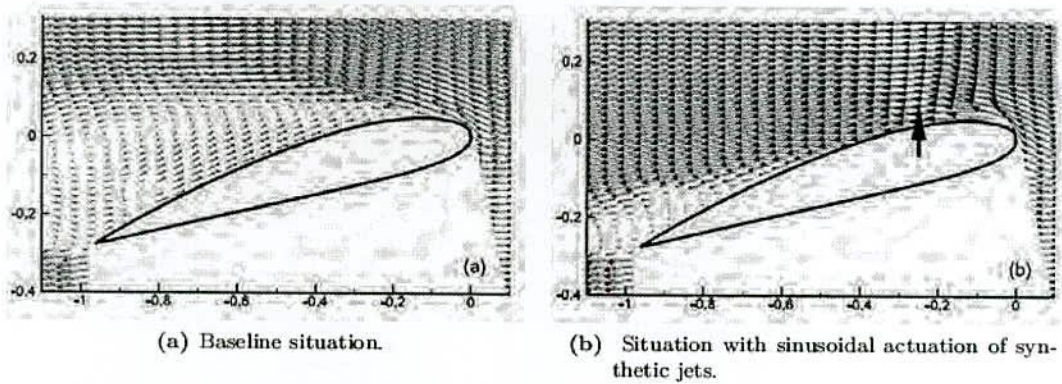


Fig. 2.1.1.2: PIV visualization of flow separation postponement on a wind turbine blade by applying synthetic jets at $\alpha = 16^\circ$ and $Re = 1.6 \cdot 10^5$. Figure from Maldonado et al. [2010].

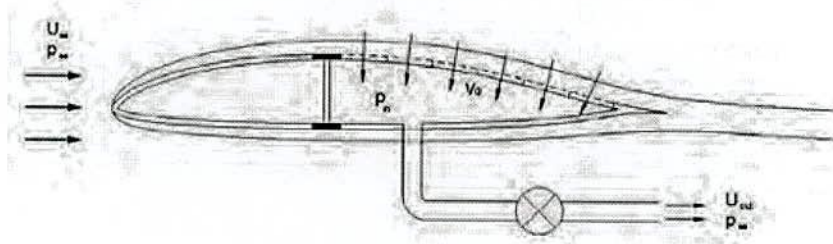


Fig. 2.1.1.3: Working principle of boundary layer suction. Figure from Boermans [2008]

Moving object/surface actuators

There are several types of moving object/surface actuators, but the most common is the piezoelectric flap. An AC-voltage across the piezoelectric device causes the flipping motion of the flap, which then interacts with the flow. In this way vortices can be created in different sizes and direction depending on the geometry and orientation with respect to the local free stream flow. A typical example of a cavity-type piezoelectric flap is shown in figure 2.1.1.4.

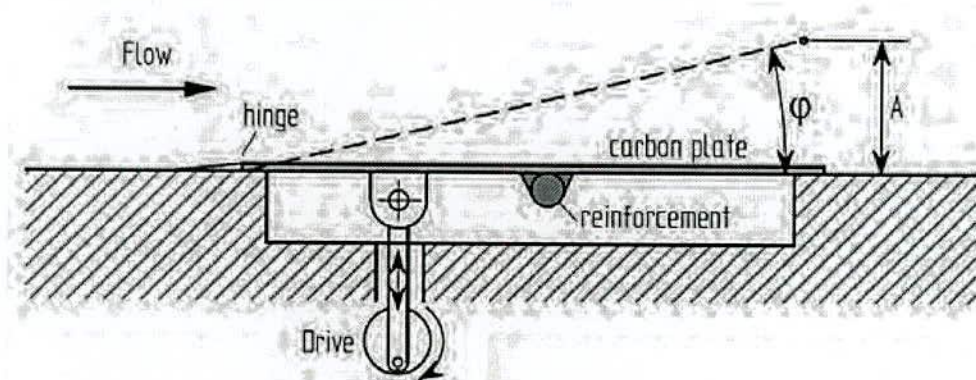


Fig. 2.1.1.4: Schematization of a piezoelectric flap. Figure from Veldhuis and van der Jagt [2010].

Plasma actuators

Plasma actuators come in different forms, having slightly different techniques to obtain the plasma. The most popular variant is the Dielectric Barrier Discharge (DBD) plasma actuator, which consists of two electrodes that are separated by a dielectric material. The air passing the electrodes becomes ionized by the voltage that is applied. The ionized air, now called plasma, produces forces in the air due to the attained electric field gradients by the electrodes. These forces can induce velocity components to the flow and thus can be used for effective flow control including delay of flow separation. Figure 2.1.1.5 shows the general setup of a DBD plasma actuator. The general advantages of plasma actuators with other active control techniques are that they are easily applicable and very compact, which gives a lot of design freedom. The main evident disadvantage is the amount of energy necessary to supply a high voltage to the electrodes.

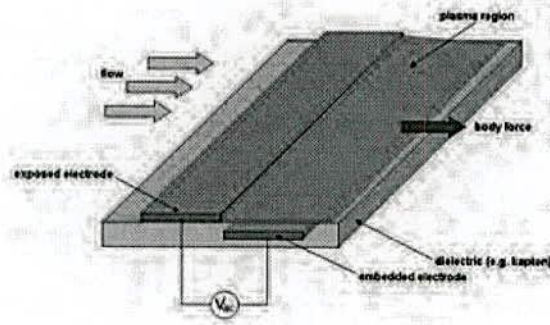


Fig. 2.1.1.5: Schematization of a DBD plasma actuator. Figure from LeBeau [2007].

2.1.2 Passive flow separation control techniques:

There are various forms of passive flow separation control techniques [16]. Unlike active flow control no direct energy is brought into the system, meaning that passive flow control is solely based on mixing high momentum fluid to areas of low momentum, hence to boundary layers which are on the verge of separation.

Vortex generators

Vortex generators (VG's) are the most commonly known passive control devices and are already used in different industries. Although VG's come in various shapes and sizes, in general a vortex generator is build up as a small vertical plate positioned at an angle with respect to the local free stream flow. With appropriate dimensioning and positioning stream wise vortices can be created which can be used to control the flow. Vortex generators can be classified in different ways. First there exist co-rotating and counter-rotating types, depicted in figure 2.1.2.1, where in general better results are obtained with the latter. Then there also exists a segmentation in terms of scale, hence conventional boundary layer VG's and more recently the development of sub-boundary layer VG's, also called micro vortex generators. Research in sub-boundary layer VG's as performed by Lin [1999] show significant improvements in reducing flow separation comparable to their larger conventional counterparts without the effects of increased drag. The counter-rotating micro VG's led to lift increases up to 10% on a leading and trailing edge flapped airfoil at accompanying drag

reductions of 50%. This was achieved by a delay in the separation location from approximately 45% flap chord to at least 85% flap chord.

In general the interest in micro VG's and creation of small-scale perturbations is quite similar to the trend found in the field of active flow control techniques. Micro VG's as other small-scale flow control solutions have a small bandwidth and the location of separation needs be somewhat fixed in order for the micro VG's to be effective.

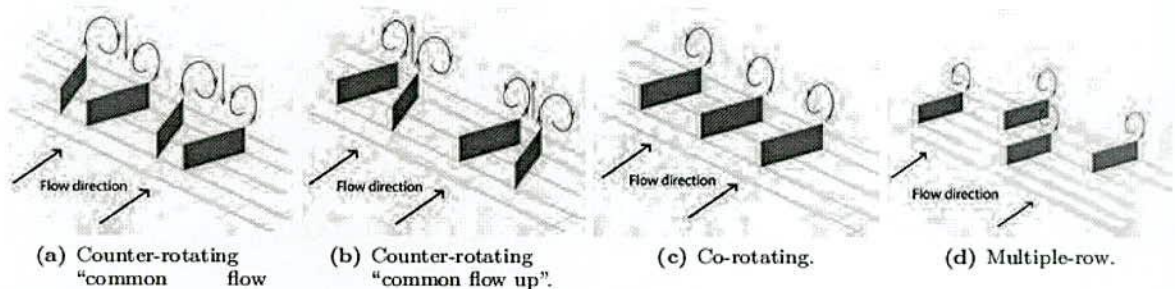


Fig. 2.1.2.1: Vortex generators displayed in different setups. Figures from von Stillfried et al. [2010].

Lift-enhancing tabs

Lift-enhancing tabs or Gurney flaps are small 'plates', which are located generally at trailing edges of lift generating devices. A typical Gurney flap is several boundary layers in height and is usually positioned perpendicular to the flow.

Figure 2.1.2.2 shows the working principle of lift-enhancing tabs. Two counter rotating vortices are created aft of the Gurney flap, entraining the flow from the airfoil upper surface around the top recirculation region. Hence the flow stays attached over the airfoil flap surface and separation can be delayed. Ashby[1996] found promising results, where various tabs on both the main airfoil and trailing edge flap were tested. Lift increases up to 11% were found at some angle of attack, while the maximum lift coefficient gained 3% with respect to the baseline configuration.

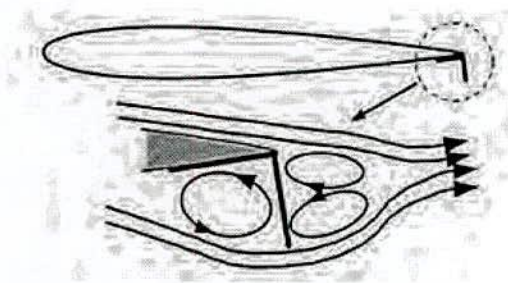


Fig. 2.1.2.2: Lift-enhancing tabs as used by Lee et al.

Even more active and passive flow separation control techniques exist and in general it can be said that very interesting results are obtained with various designs. In general active flow control techniques share the main similar disadvantage. Whether it is applying an AC-current or voltage as for the synthetic jets and plasma actuators, or fluid being blown into the system by a pump with boundary layer blowing, significant amount of energy needs to be put into the system. Often problems are encountered with the practical implementation of these mechanisms. Parts of these problems are alleviated by a migration of the active flow control research field in terms of approach, as discussed by Cattafesta [2011]. Increased flow physics understanding changed the concept from inducing large vortices to the system to focus on creating smaller instabilities to the flow. This makes it feasible to reduce power, size and mass. However for high-speed applications these 'small-scale' devices currently still lack bandwidth and often have control related issues. With passive flow control, designs are often easier applicable and design aspects like size, mass and maintenance are concept wise less an issue.

Also facets like costs and safety are considered to be less problematic for passive flow control solutions. This is the reason why passive techniques like vortex generators can already be found on various recent aircraft designs. This makes passive control very if not more interesting for the near future.

2.1.3 Co-flow jet airfoil concept:

This is an active separation control technique. Unlike the conventional circulation control airfoils, for which the jets are mostly implemented at leading and trailing edge, the co-flow jet (CFJ) airfoil is implemented on the majority area of the suction surface of the airfoil. The co-flow jet airfoil is to open a long slot on the airfoil suction surface from near leading edge to near trailing edge (see fig.2.1.3.1). A high energy jet is then injected near the leading edge tangentially and the same amount of mass flow is sucked away near the trailing edge. The turbulent shear layer between the main flow and the jet causes a strong turbulence diffusion and mixing, which enhance the lateral transport of energy and allow the main flow to overcome the severe adverse pressure gradient and stay attached at high angle of attack (AOA). At a certain AOA, the airfoil always achieves a significantly higher lift due to the augmented circulation. The operating range of AOA, hence the stall margin, is also significantly increased. The co-flow jet airfoil does not rely on the Coanda effect at the leading or trailing edge, and hence the thick leading or trailing edges are not required. The technique can apply to any type of airfoils including the modern high speed thin airfoil, and can be combined with other flow control techniques.

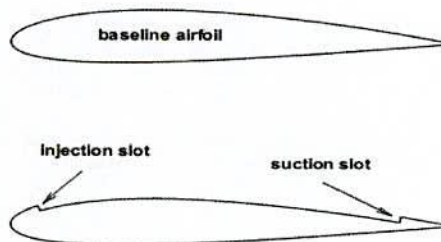


Fig. 2.1.3.1: Baseline airfoil and the air-foil with co-flow jet slot.

CHAPTER THREE

Model Design AND Model Construction

3.1 Model Design:

Co-flow jet airfoil (CFJ) geometry is slightly different from the conventional airfoil. The numbering system for CFJ is defined first to construct the model. Here we carry our investigation on an airfoil which is modified from NACA0015. The airfoil nomenclature and design is given below.

(i) Airfoil Nomenclature:

The cross-sectional shape obtained by the intersection of the wing with the perpendicular plane is called an airfoil. The major design feature of an airfoil is the mean camber line, which is locus of points halfway between the upper and lower surfaces, as measured perpendicular to the mean camber line itself. The most forward points of the mean camber line are the leading and trailing edges, respectively. The straight line connecting the leading and trailing edges is the chord line of the airfoil, and the precise distance from the leading to the trailing edge measured along the chord line is simply designated the chord of the airfoil, given by the symbol c . The camber is the maximum distance between the mean camber line and the chord line, measured perpendicular to the chord line. The camber, the shape of the mean camber line, and to a lesser extent, the thickness distribution of the airfoil essentially controls the lift and moment characteristics of the airfoil.

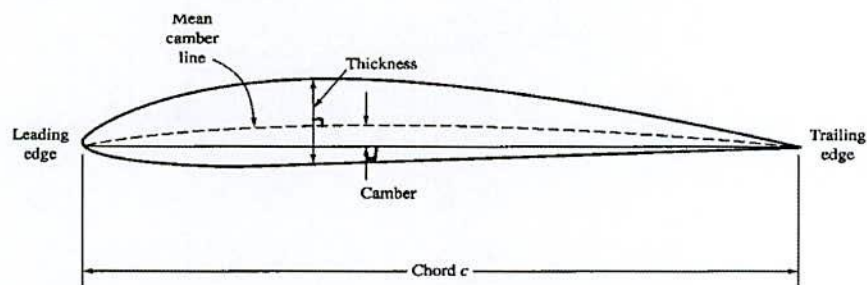


Fig.3.1.1: Airfoil nomenclature.

The numbering system for NACA 4-Digit airfoil is defined by:

NACA mpXX

Where,

XX is the maximum thickness, t/c , in percent chord.

m is the maximum value of the mean line in hundredths of chord,

p is the chord wise position of the maximum camber in tenths of the chord.

Note that although the numbering system implies integer values, the equations can provide 4 digit foils for arbitrary values of m, p, and XX.

(ii) CFJ Airfoil Geometry:

The co-flow jet airfoils are defined using the following convention: CFJ4dig-INJ-SUC, where 4dig is the same as NACA4 digit convention, INJ is replaced by the percentage of the injection slot size to the chord length and SUC is replaced by the percentage of the suction slot size to the chord length. For example, the CFJ0015-065-065 airfoil has an injection slot height of 6.5% of the chord and a suction slot height of 6.5 % of the chord. The suction surface shape is a downward translation of the portion of the original suction surface between the injection and suction slot. The injection and suction slot are located at 6.72% and 88.72% of the chord from the leading edge. The slot faces are normal to the suction surface to make the jet tangential to the main flow.

The cambered airfoil and CFJ0015-065-065 airfoil are tested in the wind tunnel tests.

(iii) Airfoil Design:

Conventional NACA4 digit airfoil is designed by following steps:

1. Pick values of x from 0 to the maximum chord c.
2. Compute the mean camber line coordinates by plugging the values of m and p into the following equations for each of the x coordinates.

$$y_c = \frac{m}{p^2}(2px - x^2) \quad \text{from } x = 0 \text{ to } x = p$$

$$y_c = \frac{m}{(1-p)^2}[(1-2p) + 2px - x^2] \quad \text{from } x = p \text{ to } x = c$$

Where

x = coordinates along the length of the airfoil, from 0 to c (which stands for chord, or length)

y = coordinates above and below the line extending along the length of the airfoil, these are either y_t for thickness coordinates or y_c for camber coordinates

t = maximum airfoil thickness in tenths of chord

m = maximum camber in tenths of the chord

p = position of the maximum camber along the chord in tenths of chord

3. Calculate the thickness distribution above (+) and below (-) the mean line by plugging the value of t into the following equation for each of the x coordinates.

$$\pm y_t = \frac{t}{0.2} (0.2969\sqrt{x} - 0.1260x - 0.3516x^2 + 0.2843x^3 - 0.1015x^4)$$

4. Determine the final coordinates for the airfoil upper surface (x_u, y_u) and lower surface (x_l, y_l) using the following relationships.

$$x_U = x - y_t \sin \theta$$

$$y_U = y_c + y_t \cos \theta$$

$$x_L = x + y_t \sin \theta$$

$$y_L = y_c - y_t \cos \theta$$

$$\text{where } \theta = \arctan \left(\frac{dy_c}{dx} \right)$$



3.2 Model Construction:

Here two types of models are prepared.

- a) Conventional airfoil model
- b) CFJ model

(a) Conventional airfoil:

Designing NACA 0015 model by using surface profile equations.

For NACA 0015,

Chord of the airfoil, $c = 0.3$ m

Maximum wing thickness, $t = \text{last two digit} \times \% c$

$$= 15 \times \frac{1}{100} \times 0.3$$

$$= 0.045$$

Maximum camber, $m = \text{first digit} \times \% c$

$$= 0 \times \frac{1}{100} \times 0.3$$

$$= 0$$

Distance from leading edge to maximum wing thickness, $p = \text{second digit} \times 10\% c$

$$= 0 \times \frac{10}{100} \times 0.3$$

$$= 0$$

Maximum wing thickness,

$$y_t = t \times (1.4845 \sqrt{x} - 0.6300 x - 1.7580 x^2 + 1.4215 x^3 - 0.5075 x^4)$$

The mean chamber line,

$$y_c = \frac{m}{p^2} (2px - x^2) \quad \text{For } 0 < x < p$$

$$\text{And, } \frac{dy_c}{dx} = \frac{2m}{p^2} (p - x)$$

$$y_c = \frac{m}{(1-p)^2} [1 - 2p + 2px - x^2] \quad \text{For } p \leq x \leq c$$

$$\text{And, } \frac{dy_c}{dx} = \frac{2m}{(1-p)^2} (p - x)$$

Now, coding a C-program including above equation and the upper and lower surface equation and after compiling this program we get a set of data for the desired airfoil. Plotting these data on any data plotting software will give the airfoil profile. The C-program used in this thesis is attached last. The obtained NACA 0015 airfoil profile is given below.

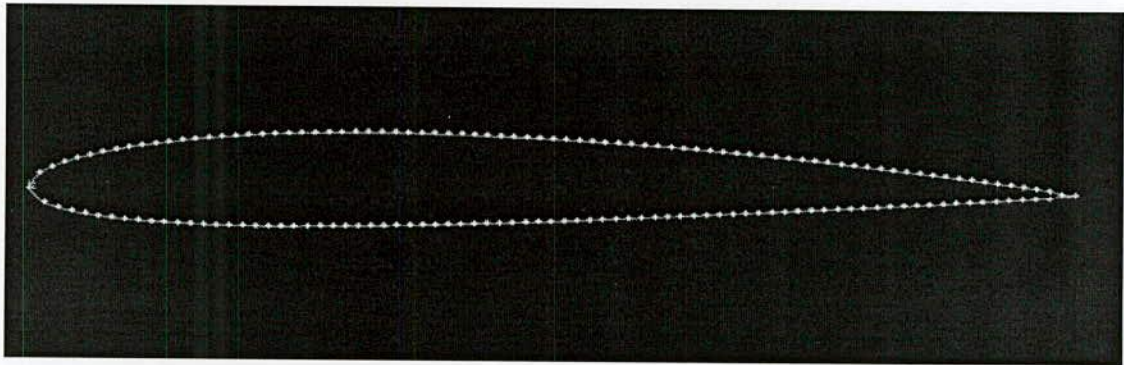


Fig.3.2.1: NACA 0015 airfoil profile

CFJ design:

The selected CFJ for performance investigation is CFJ 0015-065-065. That means it has suction and injection slot of length 6.5% of chord. The distance of the slot from the leading edge of the airfoil is taken as 6.72% of chord for injection slot and 88.62% of chord for suction slot. The profile of CFJ is simple obtained from the conventional equations for NACA 4 digit airfoil as discussed earlier with some simple modification in the equation of upper and lower surface. This modification is given below.

The equation of upper surface:

For $x \leq 0.0672$ and $x \geq 0.8872$ $x_u = x - y_t(x) \sin \theta$

And, $y_u = y_c + y_t(x) \cos \theta$

For $0.0672 \leq x \leq 0.8872$

$x_u = x - y_t(x) \sin \theta$

And, $y_u = y_c + y_t(x) \cos \theta - 0.0065$

Others equations are remain same. The C-program for generate data for CFJ is attached last. The obtained CFJ 0015-065-065 airfoil profile is given below.

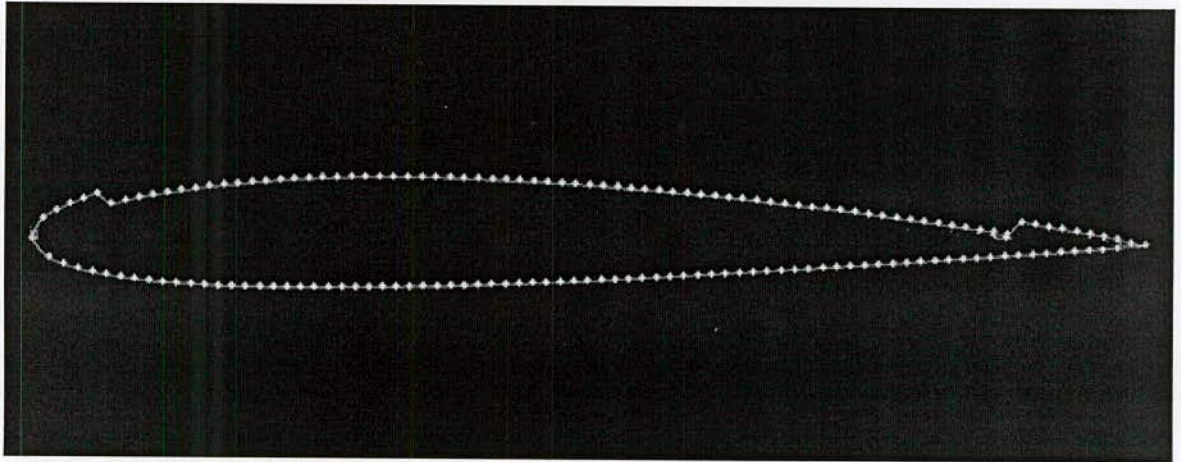


Fig. 3.2.2: CFJ 0015-065-065 airfoil.

CHAPTER 4

APPARATUS MODIFICATIONS AND ASSEMBLY

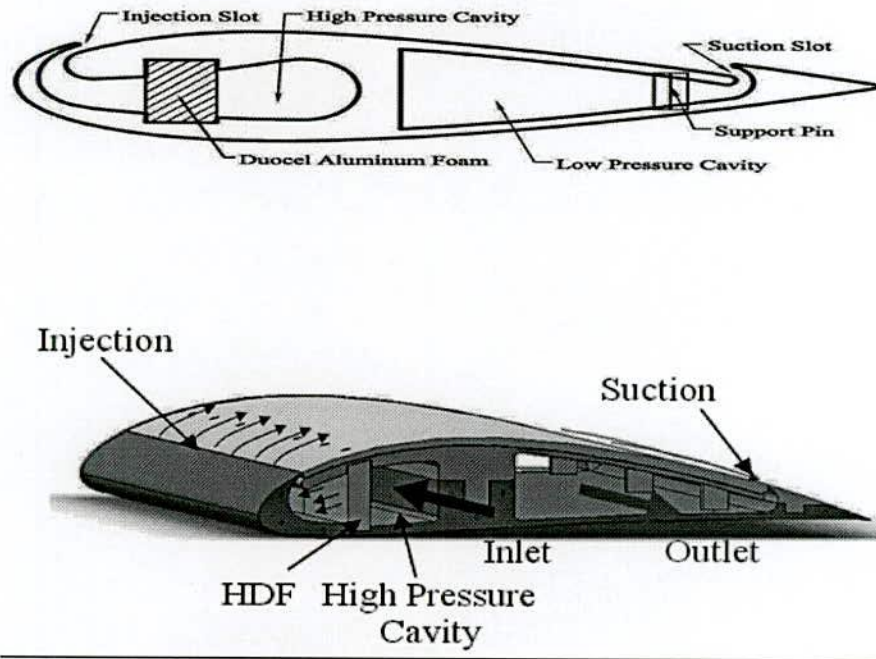
This chapter is dedicated to the description of the CFJ airfoil and the modifications made to the existing systems to enable testing of the CFJ airfoil. This section will also include the instrumentation and measurement techniques used in the wind tunnel experiments.

4.1 Co-Flow Jet Airfoil Description

The CFJ airfoils used in testing at KUET were a modified NACA 0015. The NACA 0015 airfoil was chosen for its ease of manufacturing and relative thickness. The thickness made it easier to fit all instrumentation and duct work into the airfoil given the size constraints imposed by the one-foot by one-foot wind tunnel test section; however the CFJ concept can be implemented on any airfoil geometry.

The modified NACA 0015 airfoil used in testing had a span of 0.5m and a chord length of 0.3m. As shown in figure 2-1, the airfoil was modified by recessing the suction surface (upper surface). This recession opened up a slot towards the leading edge of the airfoil (injection slot) and another slot towards the trailing edge (suction slot). The slot towards the leading edge was used to inject air tangentially over the suction surface, while the slot towards the trailing edge was used to remove air tangentially from the suction surface. One modified airfoil CFJ NACA 0015 and one Basic Airfoil NACA 0015 were tested. The injection slot and suction slot of Modified airfoil CFJ NACA 0015 had the same slot height which is 0.195 m or 0.65% of chord length. The airfoils are named by their injection and suction slot sizes according to the convention CFJ4digit-INJ-SUC. So the airfoil with the 1mm injection slot was named CFJ0015-065-065.

The reason the suction slot size was larger than the injection slot is because the density of the air being removed by the suction slot is less than the density of the air being injected. Therefore, to balance the mass flow rates, the suction area has to be larger or the velocity greater. But the velocity is limited because the flow will eventually become choked.



CFJ0015-065-065

Figure 4.1: 2-D and 3-D cross section of CFJ airfoil

The location of the injection slot and suction slot are respectively, 7.11% and 83.18% of the chord length from the leading edge. The slots are positioned perpendicular to the suction surface making them parallel to the flow direction. The support pins shown in figure 2-1 are to reinforce the suction surface of the airfoil because computer simulations indicated the suction surface might deflect in that area. The Duocel aluminum foam is used to create a backpressure in the high-pressure cavity ensuring an even distribution of air across the suction surface.

4.2 Wind Tunnel Modifications

An open loop Aerolab wind tunnel was used to test the CFJ airfoils. The wind tunnel has a test section of 1m x 1m and has an operating speed from 0-40 m/s (0-145 miles per hour). This is made possible by a 10-horse power motor that drives a fan. Figure 4.2: shows a picture of the unmodified Aerolab wind tunnel.

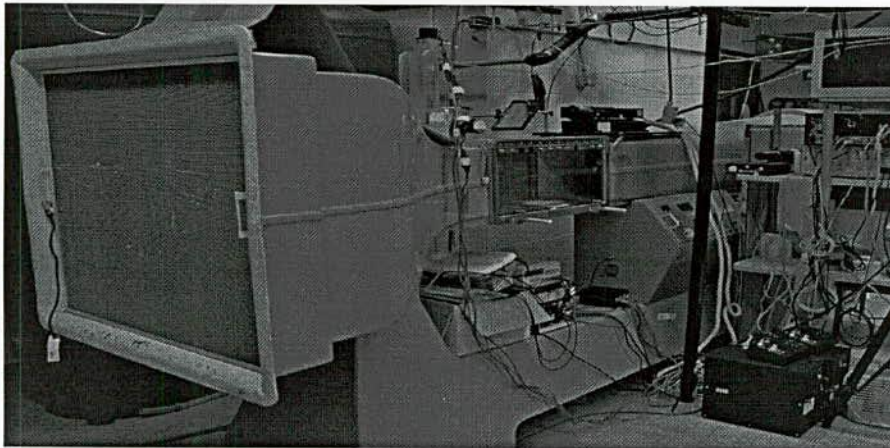


Figure 4.2: Unmodified Aerolab wind tunnel

In order to operate the injection and suction of the CFJ airfoils, many modifications had to be made to the existing Aerolab wind tunnel. The wind tunnel had to be equipped with a system to inject the desired mass flow of air. The tunnel also needed the capability to remove the air from the suction slot of the airfoil. Injecting air through the sting balance that supports the airfoil in the wind tunnel and building a Plexiglas box on the opposite side overcame these two problems. Figure 4.3 shows the modified Aerolab wind tunnel.

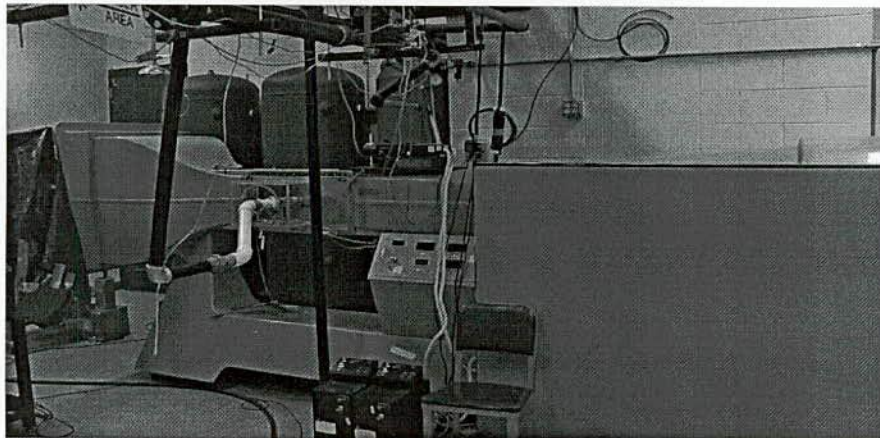


Figure 4.3: Modified Aerolab wind tunnel

An existing sting balance used to measure lift and drag forces was modified for the new wind tunnel needs. The balance is discussed in more detail later in the chapter. The cylinder of the balance, which attaches the airfoil to the rest of the balance, was

lengthened so it would completely pass through the mounting components of the balance. With the extension, there was room to attach a pressure hose and clamp (figure 4.4 shows the hose/clamp and cylinder attachment). Compressed air is then forced through the hollow cylinder into the airfoil where it passes through porous aluminum foam and is injected tangentially over the airfoil (the connection between the balance cylinder and the airfoil can be seen in figure 4.5). The foam creates backpressure and ensures uniform distribution of air across the span of the airfoil.

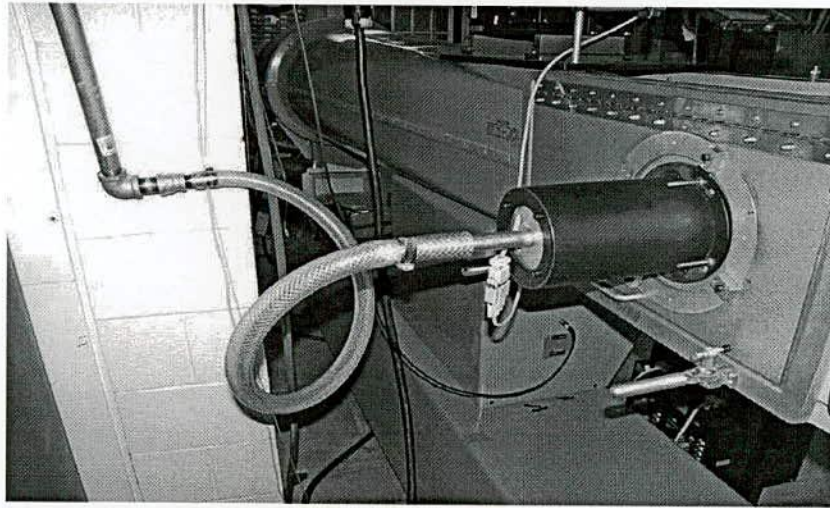


Figure 4.4: Hose/clamp attachment to cylinder and balance mechanism. Airfoil is attached in horizontal position inside tunnel.

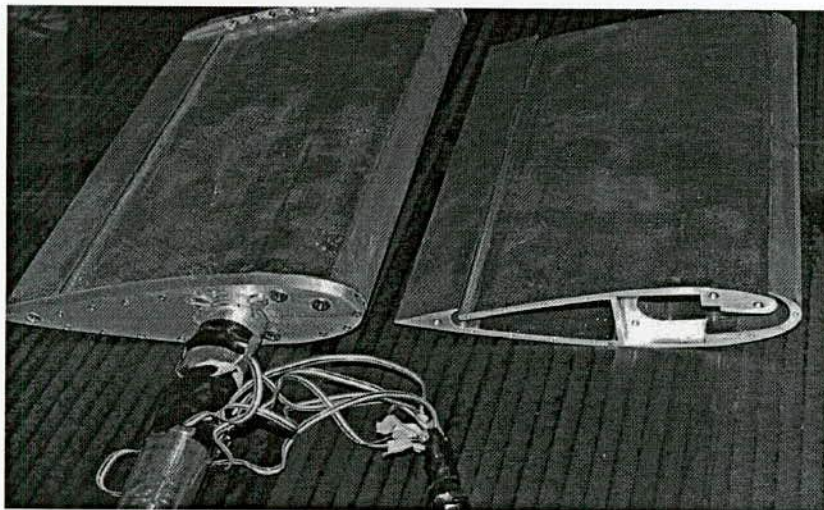


Figure 4.5: Connection between the balance cylinder and the airfoil

The opposite side of the wind tunnel originally had a flat Plexiglas wall. This was removed in order to accommodate the suction system. A suction manifold was installed on this side of

the airfoil (figure 2-6 shows the connection between the suction manifold and the airfoil). The manifold extends beyond the limits of the test section. A Plexiglas box was designed to encompass the manifold. The outside of the box was sealed as to let air leak into the test section. The inside circular wall of the box was cut out around the manifold and stagnation pressure probe (figure 4.7 show the circular wall and suction manifold inside of the Plexiglas box). The circular wall allowed enough clearance to accommodate any deflections of the airfoil from the lift and drag forces. If the airfoil deflected into the wall, some forces would be imposed onto the wall; therefore the lift and drag measurements would not be accurate.

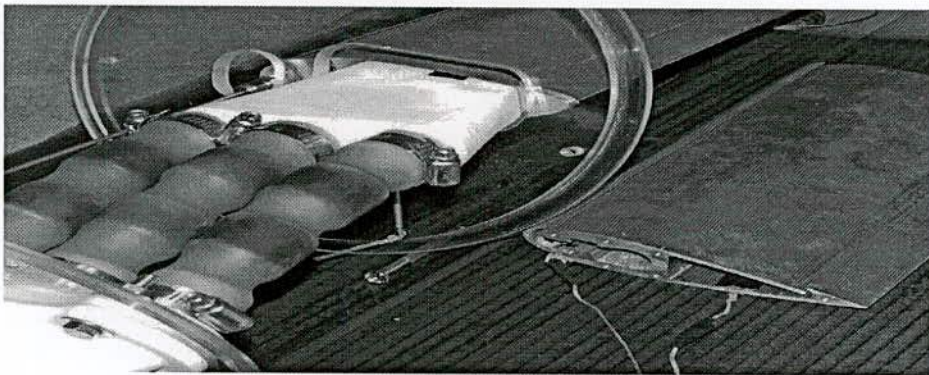


Figure 4.6: Connection between the suction manifold and the airfoil

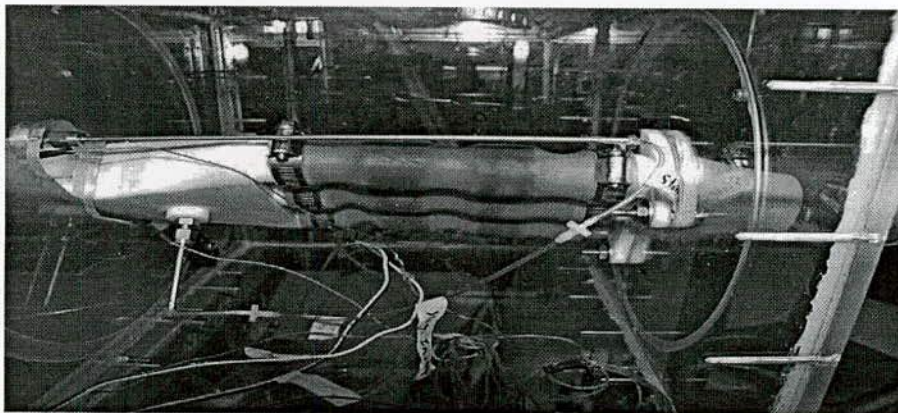


Figure 4.7: Plexiglas box and suction manifold with airfoil located to the left and external suction connection to the right

4.3 Mass Flow Rate Controls

The enhanced performance of the CFJ airfoil comes from the air that is injected at the leading edge and removed at the trailing edge; therefore it is critical to control the injection and

suction mass flow rates of air. The two mass flow rates were controlled in different manners due to the different systems available at the time of testing. A compressor supplied the air that was injected at the leading edge. The amount of air that passes through the injection slot is much less than the capability of the compressor. Therefore the stagnation pressure is always constant. A wheel valve is used to control the air flow rate so that the injection mass flow rate is remaining constant which is measured and observed by a flow meter gauge.

The suction mass flow rate was designed entirely different. The facilities at KUET did not include a vacuum pump designed to displace a large volume of air. Two vacuum pumps were available but they were designed to obtain a low pressure and hold it; to solve the problem, a high capacity vacuum pump was added onto the existing system.

The addition of the new vacuum pump solved the vacuum pump deficiency; however the mass flow rate still needed to be controlled. The idea of choking the pipe prior to the vacuum tanks was chosen as the solution. A two-valve system was designed to accomplish this. The first valve was to open and close the pipe. This valve can be thought of as an on/off switch and was always in the fully open or fully closed position. The second valve, located closer to the vacuum tanks, was used to control the mass flow rate. This valve was a gate valve. A gate valve was chosen because of the greater accuracy in adjusting the effective flow area. Since the upstream stagnation pressure is constant, the inside area of the pipe is the only variable that effects the mass flow rate.

The vacuum system must always be used in a choked condition to have a constant mass flow rate. The requirement for a choked system is the ratio of static pressure downstream of the valve to the stagnation pressure upstream of the valve to be less than 0.5283. So the system could only run until this requirement was no longer met.

The injection and the suction mass flow rates were measured using orifice plates. Equation 2-1 relates the mass flow rate to the differential pressure across the orifice plate and the upstream density. Table 2-1 gives values for all constants in equation 2-1.

$$q_m = \frac{CE\varepsilon\pi d^2 \sqrt{2\rho_1\Delta p}}{4}$$

Eqn 2-1

where,

q_m	Mass flow rate
C	Discharge coefficient
$E = \frac{1}{\sqrt{1-\beta^4}}$	Velocity approach factor
D	Inner pipe diameter
β	Ratio of orifice diameter to inner pipe diameter
ε	Gas expansion factor
d	Orifice diameter
ρ_1	Upstream density
Δp	Differential pressure across orifice plate

Table 4.1: Orifice plate 1494 coefficients

Coefficient	Injection Side	Suction Side
C	0.6079	0.6117
E	1.048	1.111
ε	0.9949	0.9659
d	1.682 in	2.026 in

The differential pressure was measured from the flanges housing the orifice plate. The upstream density was found by measuring the upstream temperature and pressure. Once the temperature, T , and pressure, P , were found, the density was obtained from the ideal gas law given in equation 2-2 with R being the gas constant for air.

$$\rho = \frac{P}{RT} \quad \text{Eqn 2-2}$$

A 0-50 inH₂O differential pressure transducer was used to measure the differential pressure across the orifice plate. Only one 0-50 inH₂O differential pressure transducer was available at the time of testing. Therefore it was impossible to measure two different mass flow rates simultaneously. A manual switch was implemented to go back and forth from measuring the injection and suction mass flow rates.

4.4 Balance Modifications

The balance used to measure lift and drag forces in the Aerolab wind tunnel was modified from a balance previously designed at the University of Florida. The main features of the balance will be described here. For an in-depth description of the balance and the calibration of the balance, the author refers the reader to reference 14.

The balance was designed in such a way that when the angle of attack is changed, the airfoil does not cause a severe blockage in the wind tunnel. Although at extremely high angle of attacks, some blockage effects were unavoidable. The extent of the blockage was not taken into account. The free stream velocity was calculated from the dynamic pressure of the test section upstream the airfoil.

The balance was designed in such a way that the airfoil would not deflect more than 1mm on the free end. This was to ensure the strain on the cylinder supporting the airfoil was within the limits of the strain gauges (where lift and drag measurements are taken). In experiments, this 1mm deflection was exceeded. The deflection of the CFJ airfoil is estimated to be 3mm; however exceeding this design parameter is not a concern.

The deflection is still small enough to allow for a small angle approximation for lift and drag. That is, lift is still assumed in the normal direction to the floor of the wind tunnel test section and drag is still assumed in the direction of the free stream. More importantly, the limitations of the strain gauges were not exceeded.

The balance was designed in such a way that the wires from the strain gauges could transverse through the side of the wind tunnel while the wind tunnel itself kept an airtight seal. The wind tunnel velocity is calculated from the dynamic pressure of the tunnel, so any air leaks into the tunnel could falsify the velocity reading. If there were airflow into the tunnel, the aerodynamic performance of the test airfoil would also be jeopardized.

The basic design of the balance was kept. Compressed air was injected into the cylinder from a hose that was clamped on the free end outside the balance.

4.5 Calibration of Airfoil

The calibration of the airfoil was modified from a previous calibration procedure. The calibration procedure calibrates for lift, drag and pitching moment. However, it was later found the pitching moment was unreliable due to the latex tubes attached at the suction side of the airfoil. The calibration procedure is outlined here. A detailed calibration procedure can be found in appendix A. An appropriate angle corresponds to an angle inside the airfoil's

angle of attack margin. The CFJ was tested from 0 deg to 30 deg, so an appropriate angle would fall anywhere between these two limits.

A metal calibration bar was then attached to the end of the clamps that holds the airfoil. The various aerodynamics properties were then measured with different AOA. The whole process was then repeated for different angle of attacks. The entire calibration process was then performed again to check for repeatability in the calibration curves. The variations in calibration curves are due to imperfection in the placement of the strain gauges on the metal cylinder and bonding of the strain gauges to the metal cylinder. Other imperfections include the solder joints and minute differences in the strain gauges themselves.

4.6 Instrumentation and Measurements

This section describes the measurements took during wind tunnel testing and the instrumentation used to take the measurements. A detailed list of all instrumentation can be found in appendix B.

The wind tunnel velocity was calculated from the dynamic pressure, $0.5 \rho V^2$ of the test section. A 0-15 inH₂O differential pressure transducer was used to measure the dynamic pressure by measuring the difference between the static pressure in the test section upstream of the airfoil and the stagnation pressure in the room. The velocity was multiplied by a correction factor, found from previous experiments, to account for the losses in stagnation pressure that occur in the tunnel inlet.

The mass flow rate was calculated using equation 2-1. All the values in this equation are constants except the upstream density and differential pressure across the orifice plate. As described earlier in the chapter, the density was found by measuring the upstream temperature and pressure and the differential pressure was measured directly by a 0-50 inH₂O differential pressure transducer.

The injection velocity was also calculated and recorded in wind tunnel testing. To calculate this velocity, the ratio of the local duct area to the sonic throat area must be found. This relation can be seen in equation 2-3.

$$\frac{A}{A^*} = \frac{KP_0 A_{jet}}{q_m \sqrt{T_0}} \quad \text{Eqn 2-3}$$

where,

K	$0.040416 \frac{s\sqrt{K}}{m}$
P_0	Total pressure in injection slot
A_{jet}	Injection slot area
q_m	Mass flow rate
T_0	Total temp injection slot

Second the area-Mach number relation must be found; this was done by a linear interpolation of A/A^* and Mach number. The interpolation was incremented from Mach number 0.1 to 1 at intervals of 0.02. Once the Mach number was found, the velocity was calculated using equation 2-4.

$$v_{jet} = M \sqrt{\gamma RT} \quad \text{Eqn 2-4}$$

where,

v_{jet}	Injection velocity
M	Mach number
γ	Specific heat ratio
R	Gas constant
T	Static temperature

The jet momentum coefficient was another item calculated and recorded by the

$$C_\mu = \frac{q_m v_{jet}}{0.5 \rho_\infty v_\infty^2 S} \quad \text{Eqn 2-5}$$

where,

C_μ	Jet momentum coefficient
q_m	Mass flow rate
ρ_∞	Free stream density
v_∞	Free stream velocity
S	Airfoil surface area

The flow was assumed incompressible, so the free stream density was equal to the ambient density and the free stream velocity was equal to the wind tunnel velocity.

4.7 Uncertainty Analysis

This section is dedicated to the uncertainty analysis of all measured and calculated values. The uncertainties of the measured values are determined first. The uncertainties of the calculated values are then found using the uncertainties of the measured values.

The measured uncertainties were found using equations 2-6, 2-7 and 2-8. In the equations U represents the total uncertainty, B represents the bias uncertainty and P represents the precision uncertainty. The uncertainties of the measured values are summarized in table 4.2.

$$U = \sqrt{B^2 + (t_{v,95}P)^2} \quad \text{Eqn 2-6}$$

$$B = \sqrt{B_1^2 + B_2^2 + \dots + B_M^2} \quad \text{Eqn 2-7}$$

$$P = \sqrt{P_1^2 + P_2^2 + \dots + P_N^2} \quad \text{Eqn 2-8}$$

The calculated uncertainties were found using equations 2-9 and 2-10.

$$R = R(x_1, x_2, \dots, x_j) \quad \text{Eqn 2-9}$$

$$U_R = \sqrt{\left(\frac{\partial R}{\partial x_1} U_{x_1}\right)^2 + \left(\frac{\partial R}{\partial x_2} U_{x_2}\right)^2 + \dots + \left(\frac{\partial R}{\partial x_j} U_{x_j}\right)^2} \quad \text{Eqn 2-10}$$

Table 4.2: List of Uncertainties of the measured values

Measurement	Uncertainty
Dynamic pressure from wind tunnel	0.014 inH ₂ O
Differential pressure across orifice plate	0.134 inH ₂ O
Static pressure in injection pipe	0.102 psi
Static pressure in suction pipe	0.092 psi
Stagnation pressure in injection slot	0.553 kPa
Static pressure in suction manifold	0.295 kPa
Static temperature in injection pipe	1.170 C
Static temperature in suction pipe	0.730 C
Static temperature in injection duct of airfoil	0.730 C
Static temperature in suction duct of airfoil	0.730 C
Lift force, C_l	0.0088-0.043
Drag force, C_d	0.0088-0.043

The wind tunnel velocity is found from the dynamic pressure. The velocity was calculated using equation 2-11.

$$v = \sqrt{\frac{2q}{\rho}} \quad \text{Eqn 2-11}$$

where,

v Wind tunnel velocity
 q Dynamic pressure
 ρ Density of free stream

The uncertainty in the velocity measurement reduces to equations 2-12. The uncertainty in the velocity measurement is 0.748 m/s or 2.08%. The velocity of the wind tunnel was also checked with PIV. The velocity measured from PIV was within the uncertainty.

$$U_v = \sqrt{\left(\frac{\partial v}{\partial q} U_q\right)^2 + \left(\frac{\partial v}{\partial \rho} U_\rho\right)^2} \quad \text{Eqn 2-12}$$

The mass flow rate was given by equation 2-1. The uncertainty of the mass flow rate can be reduced to equation 2-13. Table 2-3 shows values for the given uncertainties.

$$\frac{\partial q_m}{q_m} = \left[\left(\frac{\partial C}{C}\right)^2 + \left(\frac{\partial \varepsilon}{\varepsilon}\right)^2 + \left(\frac{2\beta^4}{1-\beta^4}\right)^2 \left(\frac{\partial D}{D}\right)^2 + \left(\frac{2}{1-\beta^4}\right)^2 \left(\frac{\partial d}{d}\right)^2 + \frac{1}{4} \left(\frac{\partial \Delta p}{\Delta p}\right)^2 + \frac{1}{4} \left(\frac{\partial \rho}{\rho}\right)^2 \right]^{\frac{1}{2}} \quad \text{Eqn 2-13}$$

Table 4.3: Uncertainty in orifice plate calculation

Coefficient	Uncertainty of Injection Side, %	Uncertainty of Suction Side, %
$\frac{\partial C}{C}$	0.06	0.06
$\frac{\partial \varepsilon}{\varepsilon}$	0.144	0.144
$\left(\frac{2\beta^4}{1-\beta^4}\right)^2 \left(\frac{\partial D}{D}\right)^2$	≈ 0	≈ 0
$\left(\frac{2}{1-\beta^4}\right)^2 \left(\frac{\partial d}{d}\right)^2$	≈ 0	≈ 0
$\frac{\partial \Delta p}{\Delta p}$	1.914	2.197
$\frac{\partial \rho_1}{\rho_1} = \sqrt{\left(\frac{\partial p_1}{p_1}\right)^2 + \left(\frac{\partial T_1}{T_1}\right)^2}$	0.562	0.870

The uncertainty in the mass flow rate measurement is 1.01% for the injection and 1.19% for the suction.

The uncertainty in A/A^* needs to be found before the uncertainty of the injection velocity can be determined. Equation 2-3 defined A/A^* . The uncertainty of this ratio is given in equation 2-14.

$$U_{A/A^*} = \sqrt{\left(\frac{\partial(A/A^*)}{\partial P_0} U_{P_0}\right)^2 + \left(\frac{\partial(A/A^*)}{\partial q_m} U_{q_m}\right)^2 + \left(\frac{\partial(A/A^*)}{\partial T_0} U_{T_0}\right)^2} \quad \text{Eqn 2-14}$$

The jet momentum coefficient is the last quantity for which the uncertainty needs to be calculated. The jet momentum coefficient was defined in equation 2-5. The uncertainty of the jet momentum coefficient is given by equation 2-15.

$$U_{C_\mu} = \sqrt{\left(\frac{\partial(C_\mu)}{\partial v_{jet}} U_{v_{jet}}\right)^2 + \left(\frac{\partial(C_\mu)}{\partial q_m} U_{q_m}\right)^2 + \left(\frac{\partial(C_\mu)}{\partial v_\infty} U_{v_\infty}\right)^2} \quad \text{Eqn 2-15}$$

The uncertainty of the jet momentum coefficient is calculated to be 4.59%.

The uncertainty of the lift and drag was calculated using Student's t-distribution [15], which is given in equation 2-16. Student's t-distribution gives the uncertainty of the true mean.

The uncertainty in A/A^* is calculated to be 1.37%. This relates to an uncertainty in the Mach number of 1.65%. This uncertainty relates directly to the uncertainty of the velocity because the speed of sound, a , is considered constant. So the uncertainty of the injection velocity is 1.65%.



$$\Delta = \frac{t\sigma}{\sqrt{n}}$$

Eqn 2-16

where,

Δ	Uncertainty
t	t-value for corresponding confidence level
σ	Standard deviation
n	Number of samples

For a 95% confidence level and 50 samples, the t-value is equal to 2.0105. The standard deviation for both lift and drag at lower angle of attacks is 1 N and at higher angle of attacks is 5 N. This corresponds to standard deviation in terms of C_l and C_d of 0.031-0.153. So, the uncertainty in C_l and C_d would then be 0.0088 at lower angle of attacks and 0.043 at higher angle of attacks.

CHAPTER FIVE

PROCEDURE

This chapter describes the experimental procedure followed during the testing of the CFJ airfoils. The airfoils were tested in two configurations. The CFJ0015-065-065 along with a baseline airfoil. The airfoils were also tested in two different manners. The airfoils were tested for lift and drag characteristics with strain gauges and flow field visualization with smoke generation.

The lift and drag testing is discussed first. A rigorous airfoil assembly procedure and testing procedure can be found in appendix C and appendix D respectively. The airfoil to be tested would have to be assembled and placed into the wind tunnel. Once the airfoil was in the wind tunnel, the procedure was as follows:

1. Turn on vacuum pump and begin pulling vacuum
2. Start compressor
3. Connect different probes to appropriate transducers
4. Turn on all instrumentation and computer
5. Set zero degree angle of attack
6. Rotate airfoil to desired angle of attack
7. Turn on wind tunnel
8. Start air injection
9. Dial in suction mass flow rate
10. Only continue after the suction mass flow rate is desirable
11. Start air suction and sampling
12. Measuring the pressure on different equally spaced slot in both upper camber and lower camber with the help of manometer
13. Repeat the same procedure to justify the fluctuation of uncertainty and identify the correct data.

CHAPTER SIX

DISCUSSION OF RESULTS

This chapter is dedicated to the results from the wind tunnel tests conducted at the KUET. This chapter includes tests taken for lift and drag measurements as well as tests taken for flow field visualization. The CFJ airfoil was tested in many ways. These will all be described in detail in this chapter.

6.1 Different Tests Conducted

The Modified CFJ0015-065-065 and Basic airfoils were tested in many different manners. The airfoils were tested to study things such as Pressure coefficient C_p distribution, lift, drag, stall angle, Injection Jet velocity, Jet momentum coefficient, separation due to high injection mass flow rate and effects of lift and drag due to altered mass flow rates.

Figure 6.1 is a summary of the CFJ0015-065-065 Injection Velocity with AoA at different mass flow rate.

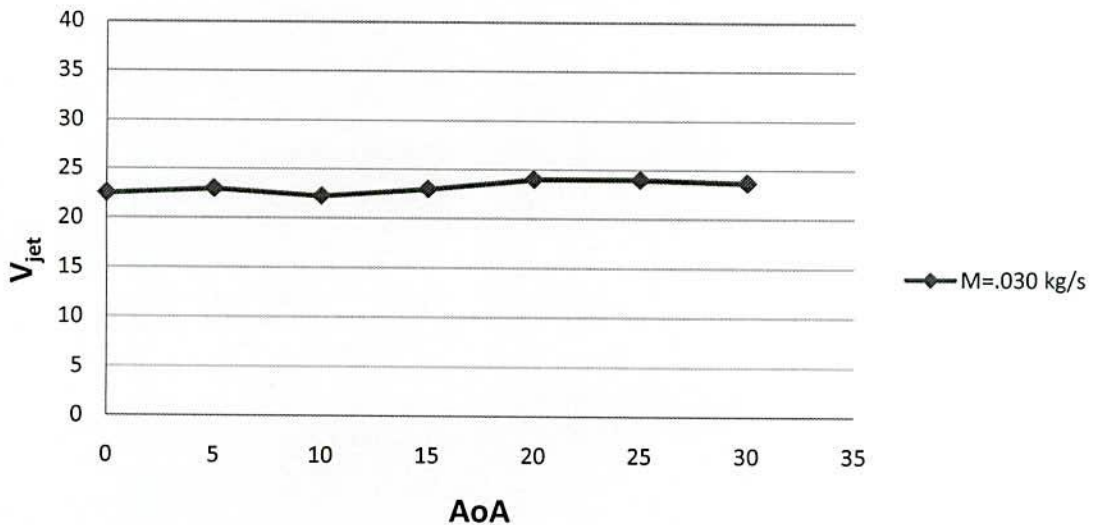


Figure 6.1: Injection Velocity vs. AoA at different mass flow rate.

It was seen that for CFJ0015-065-065 airfoil as the mass flow rate is increasing the value of Injection Velocity is also increased. The avg. value of V_{jet} is 24 m/s at $M=0.030$ kg/s.

Figure 6.2 is a summary of the CFJ0015-065-065 Drag performance.

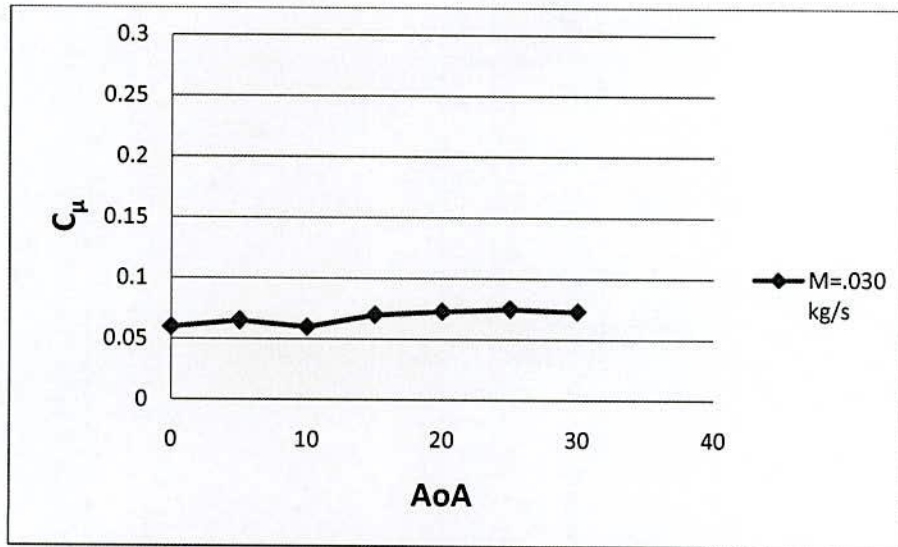


Figure 6.2: C_μ vs. AoA at Different Mass flow Rate

It was seen that for CFJ0015-065-065 airfoil as the mass flow rate is increasing the value of lower camber pressure is also increased. That is why lift is increasing abruptly with different AOA. Hence the value of C_μ is increased and shows a maximum value of 0.075 at $M= 0.030$ kg/s

The pressure distribution along the upper camber and lower camber of this Modified CFJ0015-065-065 shows the scenario that the value of C_p gradually increased in lower camber as the AoA increased. For the AoA=05 deg, the variation of C_p with respect to x/c is described in the following graph.

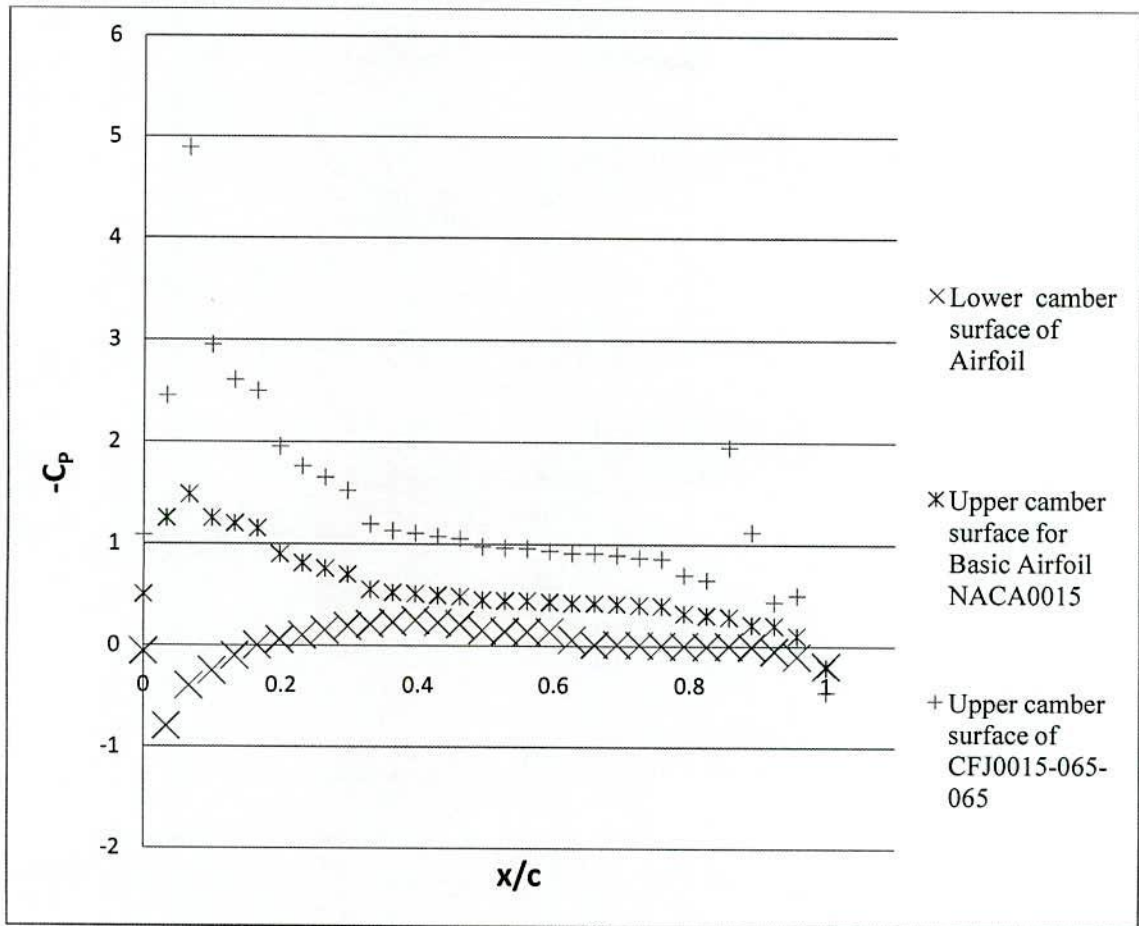


Figure 6.3: $-C_p$ vs. x/c at $AoA= 05$ deg.

From Figure 6.3 we can see that the stagnation point is indeed on the underside of the wing very near the front at $\frac{x}{c} = 0.01$. There are no flat areas of C_p which indicates that there is no boundary layer separation. It was also seen that at 05 degree AoA the pressure distribution along the chord length increased bit by bit and shows a peak in injection slot having a value of 2.90 at $\frac{x}{c} = 0.15$. The value of $-C_p$ was 1.10 at $x/c = 0.90$ in upper camber surface at suction slot. But in Baseline airfoil the pressure distribution shows a smooth variation in both upper camber surface and lower camber surface. The maximum value of $-C_p$ in Baseline Airfoil are 1.5 and 0.25 at upper camber surface and lower camber surface respectively.

For the $AoA=12$ deg, the variation of C_p with respect to x/c is described in the following graph

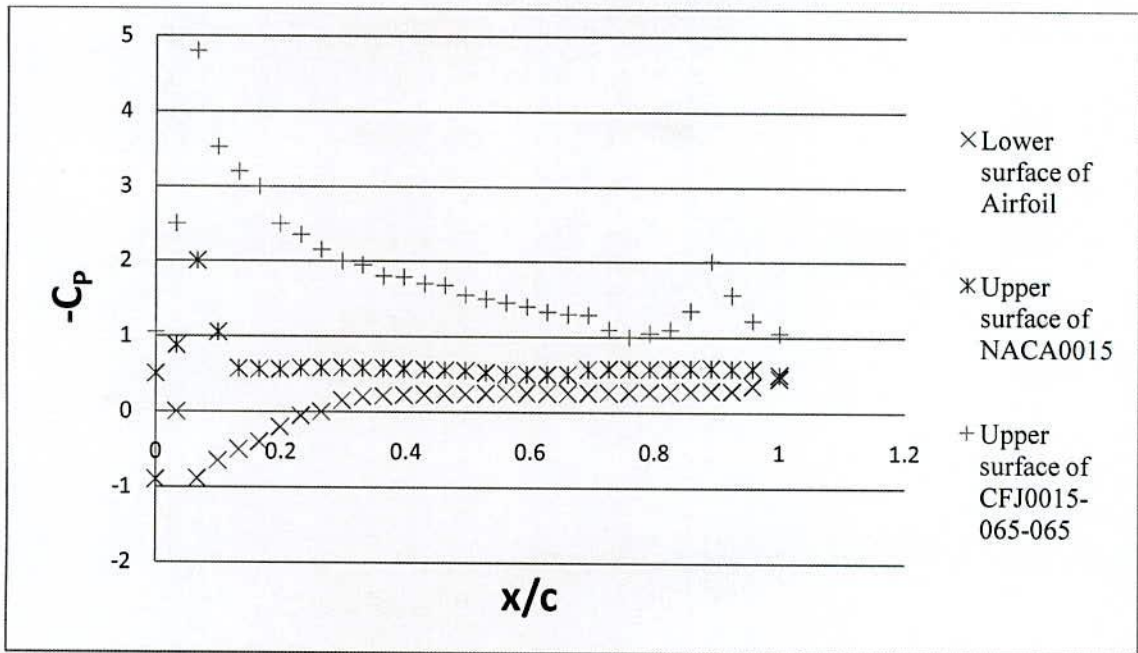


Figure 6.4: $-C_p$ vs. x/c at $AoA=12$ deg.

From Figure 6.4 we can see that the stagnation point is indeed on the underside of the wing very near the front at $\frac{x}{c} = 0.022$. There are no flat areas of C_p which indicates that there is no boundary layer separation. It was also seen that at 12 degree AoA the pressure distribution along the chord length increased bit by bit and shows a peak in injection slot having a value of 4.70 at $\frac{x}{c} = 0.10$. The value of $-C_p$ was 2.02 at $x/c = 0.90$ in upper camber surface at suction slot. But in Baseline airfoil the pressure distribution shows a smooth variation in both upper camber surface and lower camber surface. The maximum value of $-C_p$ in Baseline Airfoil are 2.0 and 0.20 at upper camber surface and lower camber surface respectively.

For the $AoA=20$ deg, the variation of C_p with respect to x/c is described in the following graph

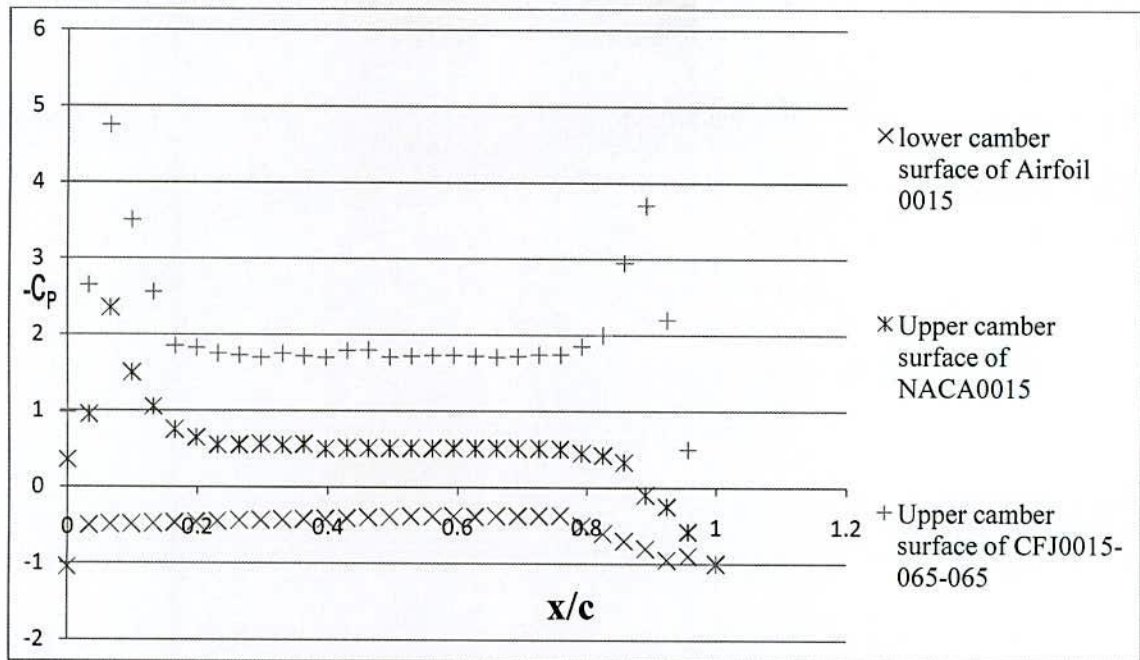


Figure 6.5: $-C_p$ vs. x/c at $AoA=20$ deg.

From Figure 6.5 we can see that the stagnation point is indeed on the underside of the wing very near the front at $\frac{x}{c} = 0.022$. There are no flat areas of C_p which indicates that there is no boundary layer separation. It was also seen that at 20 degree AOA the pressure distribution along the chord length increased bit by bit and shows a peak in injection slot having a value of 4.75 at $\frac{x}{c} = 0.085$. The value of $-C_p$ was 3.65 at $x/c = 0.90$ in upper camber surface at suction slot. But in Baseline airfoil the pressure distribution shows a smooth variation in both upper camber surface and lower camber surface. The maximum value of $-C_p$ in Baseline Airfoil are 2.30 and -0.50 at upper camber surface and lower camber surface respectively.

6.2 Improved Lift, Drag and Stall

During the lift and drag measurements, the stagnation pressure of the injection jet dictated the mass flow rate. For CFJ0015-065-065 and Basic airfoil, the desired mass flow rate was kept constant for $AoA=0$ deg to $AoA=30$ deg. This stagnation pressure was the pressure at which all other angles of attack were run. So, the mass flow rate did vary slightly depending on the angle of attack.

Figure 6.6 is a summary of the CFJ0015-065-065 lift performance. It can be seen that the higher mass flow rates have a higher lift coefficient and stall margin. This is not a surprising result. When the mass flow was raised, the jet momentum coefficient was raised; meaning the amount of momentum injected into the flow was higher. Also plotted is the performance of the NACA 0015 for comparison.

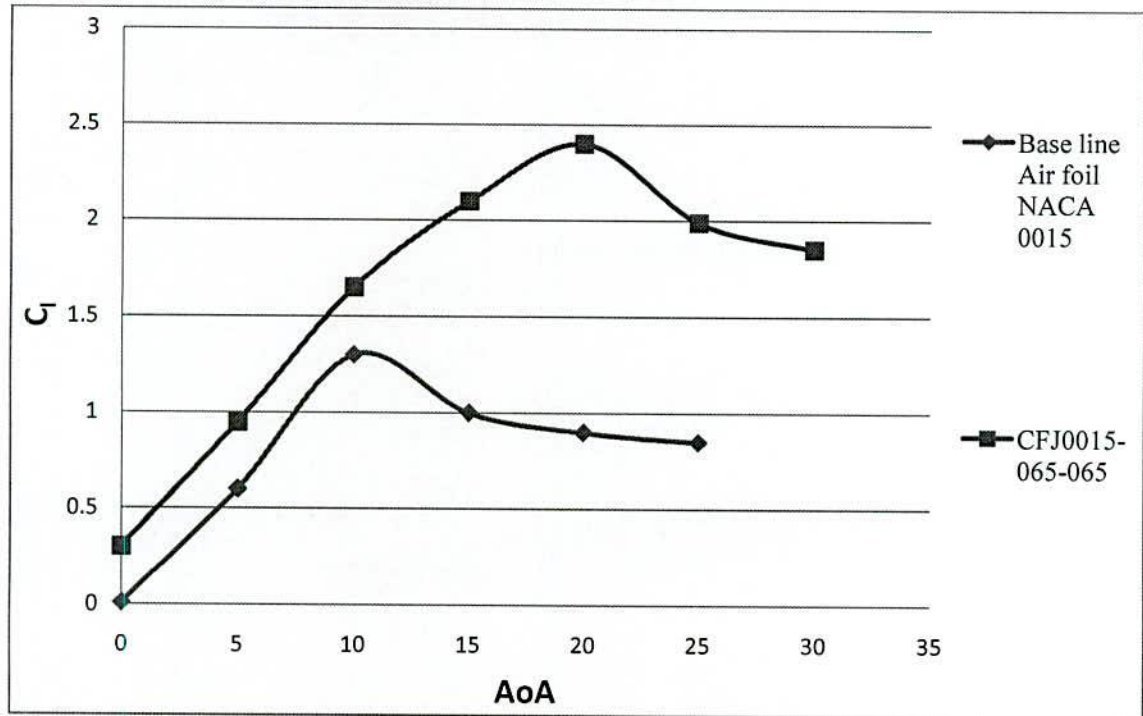


Figure 6.6: Lift coefficient verse angle of attack for CFJ0015-065-065 at $C_{\mu}=0.07$ and $Re=1.89 \times 10^5$

It was seen that at base line airfoil have $C_{l \max} = 1.65$ at stall AOA of 12 deg whereas CFJ0015-065-065 have $C_{l \max} = 2.75$ at stall AOA of 20 deg. There is a huge increase in lift coefficient which shows the high lift at high AoA and at high stall margin at $C_{\mu}=0.07$

Figure 6.7 is a summary of the CFJ0015-065-065 Drag Coefficient.

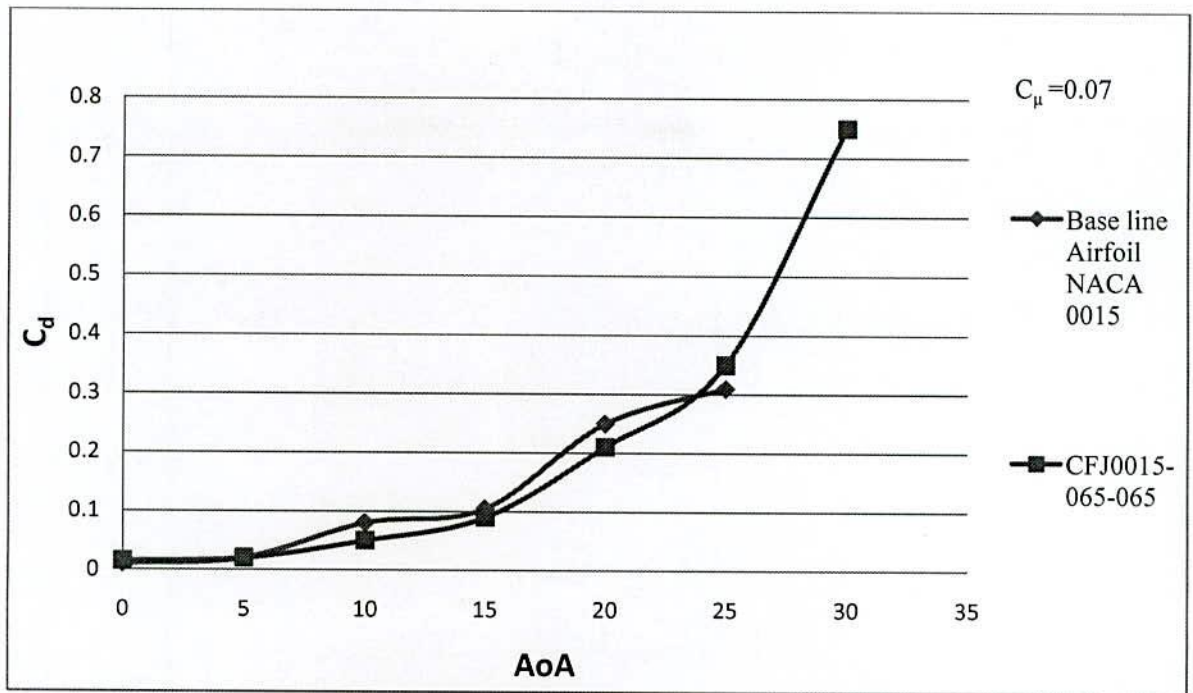


Figure 6.7: Drag Coefficient vs. AOA for CFJ0015-065-065 at $C_{\mu}=0.07$ and $Re=1.89 \times 10^5$

It was seen that at base line airfoil have $C_{l_{max}} = 0.3$ at stall AOA of 25 deg whereas CFJ0015-065-065 have $C_{l_{max}} = 0.75$ at stall AOA of 30 deg. There is a huge increase in lift coefficient which shows the high lift at high AOA and at high stall margin at $C_{\mu}=0.07$

Figure 6.8 is a summary of the CFJ0015-065-065 Drag performance.

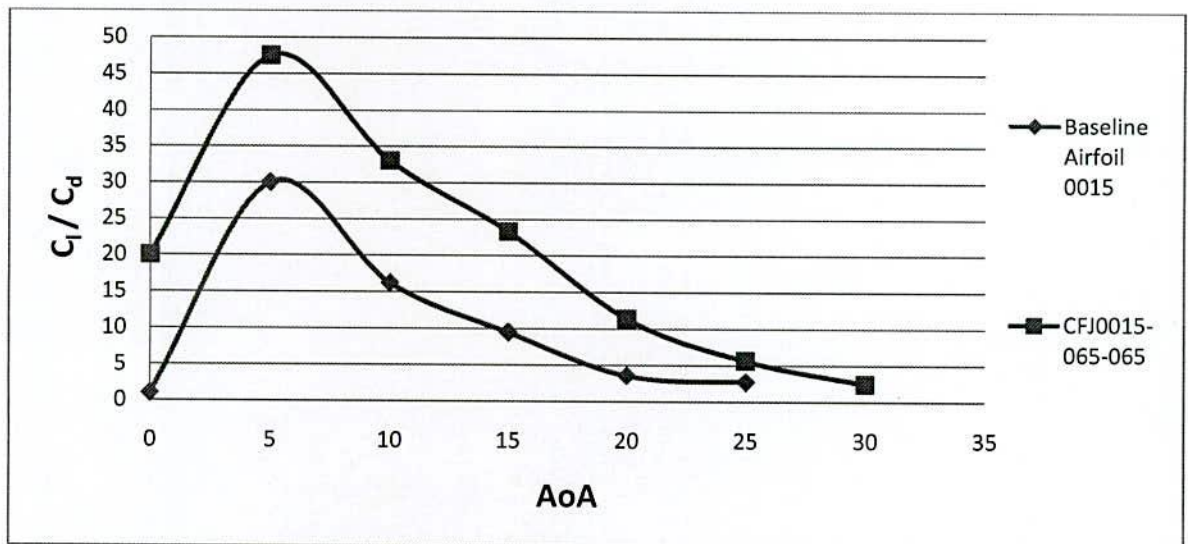


Figure 6.8: C_l vs. C_d curve at $C_{\mu}=0.07$ and $Re=1.89 \times 10^5$

It was seen that for CFJ0015-065-065 airfoil the value of C_l/C_d were raised to 47 and for the Baseline Airfoil it was 30 at 05 deg AoA and $C_{\mu} = 0.07$. Then the value of C_l/C_d gradually decreased as the AoA is increased.

6.3 Flow Visualization effect

Since it is required to see the Flow separation control phenomena at different AoA for both CFJ0015-065-065 and Base line Airfoil 0012 I was used smoke Flow Visualization technique. These are the result observed in wind tunnel section.

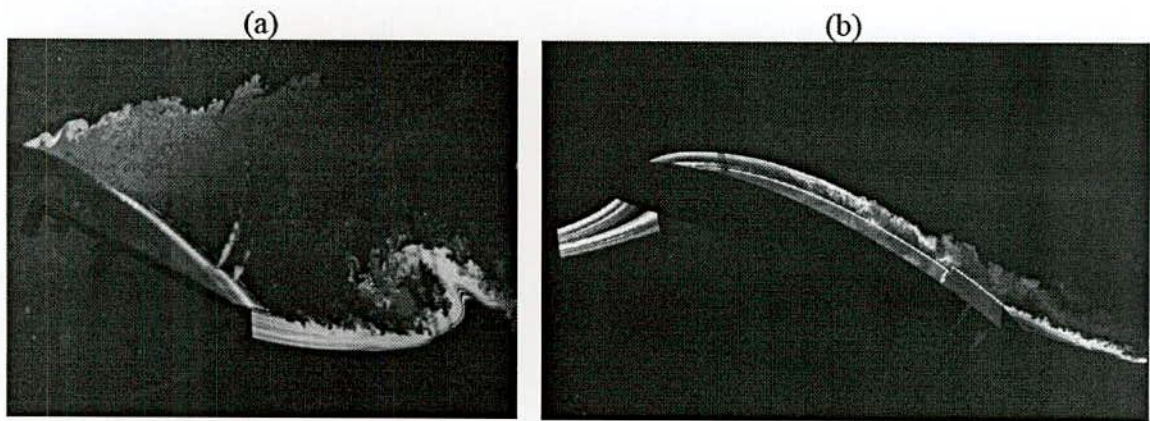


Figure 6.9: Smoke Flow Visualization for (a) Baseline and (b) CFJ ($C_{\mu} = 0.14$) at AOA = 25°

It was seen that for CFJ0015-065-065 airfoil the flow is stream line flow and flow remain attach with the periphery of Airfoil Geometry up to the near end of Trailing edge i.e. the Wake formation is controlled and delayed for certain period of time whereas the Baseline Airfoil has the minimum control over flow separation since there turbulence is created and Hence eddy is formed which detach the stream from the surface of Airfoil.

CHAPTER 5

CONCLUSION AND RECOMMENDATION

The research described in this thesis successfully demonstrated how the CFJ airfoil transitioned from CFD modeling to wind tunnel testing. The research proved the high performance capabilities of the CFJ airfoil. It was seen that the value of lift improvement are 82.5 % at Stall AoA and 49% at 0 deg AoA at $C_{\mu} = 0.07$ for CFJ0015-065-065. The Average value of V_{jet} is 24 m/s at $M = 0.03$ kg/s and it shows a steady trend over 20 to 30 deg AoA. The value of C_{μ} is 0.07 m/s at $M = 0.03$ kg/s and it shows a steady trend over 15 to 30 deg AoA. For 05 and 12 deg AoA the figure of $-C_p$ shows a gradual increase in its values and reach a peak at injection slot upto 4.56 to 4.8 and also shows a peak at suction slot having a value around 1.95. But at AoA= 20 deg, the figure shows a zigzag trend and although it has a peak both at injection and suction slots but the end values in both surface are equal. since some air is injected and sucked at a constant rate, It also seen from the graph that over the CFJ0015-065-065 model the streamlines are remain attach to airfoil surface which protect the occurrence of turbulence and hence by this jet mixing Co flow jet it is able to delay the flow separation. The value of C_l is 2.45 at 20 deg AoA for CFJ0015-065-065 Airfoil but 1.35 at 12 deg AoA for baseline Airfoil. The value of C_d is 0.35 at 25 deg AoA for CFJ0015-065-065 Airfoil but 0.30 for Baseline Airfoil.

The Values of C_l C_d are 47 and 35 for CFJ0015-065-065 and baseline Airfoil NACA0015 respectively. The value of Lift is increased, Drag is reduced and flow separation is controlled sufficiently by this project work and that was also my concern that is fulfilled by this work.

Much optimization still remains for the CFJ airfoil geometry. The geometry of the airfoil was chosen from CFD simulations. Only one injection slot sizes were tested in the wind tunnel. Many different slot heights should be tried, both for the injection and for the suction. The slot location and slot area will also have a significant effect on the performance of the airfoil. In future work, it is planned to have an injection slot that can be adjusted for both location and height.

The amount of mass injected can be controlled by a number of different means. It is not known which of these the best method to obtain the peak performance is. The mass injected can be controlled by a direct measurement of the mass flow rate. The stagnation pressure of the injection jet or the jet momentum coefficient can also control the mass injected. It might also be beneficial to control the velocity of the injection jet.

An in-depth study of the shear-mixing region would also be advantageous to the success of the CFJ airfoil. It is known the CFJ airfoil suppresses separation and increases lift from the addition of momentum and the induced mixing with the free stream. The mechanics of the turbulent shear layer mixing the free stream and the jet is largely unknown.

Future work also consists of investigating three-dimensional effects of a wing utilizing a CFJ. Work here would include looking at tip effects due to the CFJ. Other items to be looked at include the length the slots should extend towards the wingtips and if there should be any variation in the slot height or location along the wingspan. It will be shown that the smaller injection slot airfoil performed better than the larger injection slot airfoil with respect to maximum lift and stall margin. It will also be shown the larger injection slot airfoil performed better than the smaller injection slot airfoil with respect to lift for a given angle of attack and drag reduction.

REFERENCES

- [1] M. Gad-el Hak, "Flow Control: The Future," *Journal of Aircraft*, vol. 38, pp. 402-418, 2001.
- [2] M. Gad-el Hak, *Flow Control, Passive, Active, and Reactive Flow Management*. Cambridge University Press, 2000.
- [3] V. Modi, M. Fernando, and T. Yokomizo, "Drag Reduction of Bluff Bodies Through Moving Surface Boundary Layer Control." AIAA Paper No. 90-0298, 1990.
- [4] D. Cichy, J. Harris, and J. MacKay, "Flight Tests of a Rotating Cylinder Flap on a North American Rockwell YOY-10A Aircraft." NASA CR-2135, 1972.
- [5] L. C. Bradley, "An Experimental Investigation of A Sting-Mounted Finite Circulation Control Wing." M.S. Thesis, Air Force Institute of Technology, 1995.
- [6] N. Wood, L. Robert, and Z. Celik, "Control of Asymmetric Vortical Flows over Delta Wings at High Angle of Attack," *Journal of Aircraft*, vol. 27, pp. 429-435, 1990.
- [7] N. Wood and L. Robert, "Control of Vortical Lift on Delta Wings by Tangential Leading-Edge Blowing," *Journal of Aircraft*, vol. 25, pp. 236-243, 1988.
- [8] N. Wood and J. Nielsen, "Circulation Control Airfoils-Past, Present, Future." AIAA Paper 85-0204, 1985.
- [9] R. J. Englar, L. A. Trobaugh, and R. Hemmersly, "STOL Potential of the Circulation Control Wing for High-Performance Aircraft," *Journal of Aircraft*, vol. 14, pp. 175-181, 1978.
- [10] R. J. Englar, "Circulation Control for High Lift and Drag Generation on STOL Aircraft," *Journal of Aircraft*, vol. 12, pp. 457-463, 1975.
- [11] A. Smith, "High-Lift Aerodynamics," *Journal of Aircraft*, vol. 12, pp. 501-530, 1975.
- [12] J. Lin, S. Robinson, R. McGhee, and W. Valarezo, "Separation Control on High Reynolds Number Multi-Element Airfoils." AIAA Paper 92-2636, 1992.
- [13] K. McManus and J. Magill, "Airfoil Performance Enhancement Using Pulsed Jet Separation Control." AIAA Paper 97-1971, 1997.

- [14] K. McManus and J. Magill, "Separation Control in Incompressible and Compressible Flows Using Pulsed Jets." AIAA Paper 96-1948, 1996.
- [15] H. Johari and K. McManus, "Visulation of Pulsed Vortex Generator Jets for Active Control of Boundary Layer Separation." AIAA Paper 97-2021, 1997.
- [16] G.-C. Zha, (team members: David Car, and W. Copenhaver), "Super Diffusion Cascades Using Co-Flow Jet Flow Control." National Research Council Summer Faculty Final Report, Aug.23, 2002.
- [17] D. Car, N. J. Kuprowicz, J. Estevadeordal, G.-C. Zha, and W. Copenhaver, "Stator Diffusion Enhancement Using A Re-circulating Co-flowing steady Jet." ASME GT-2004-53086, ASME TURBO EXPO 2004, June 14-17, 2004.
- [18] Y. Liu, L. N. Sankar, R. J. Englar, K. K. Ahuja, and R. Gaeta, "Computational Evaluation of the Steady and Pulsed Jet Effects on the Performance of a Circulation Control Wing Section." AIAA Paper 2004-0056, 42nd AIAA Aerospace Sciences Meeting and Exhibit, Reno, Nevada
5 - 8 Jan 2004.

APPENDIX A

DETAILED CALIBRATION PROCEDURE

1. Plug in power supply and data acquisition/switch unit
2. Check the power supplies 5V output with the Multimeter to make sure the output is indeed 5V
3. Connect all appropriate connections.
4. If this calibration has already been performed and the experimentalist wants only to check the accuracy of the calibration or reading, go to step 10
5. Rigidly attach balance clamp is used to fixed object such as an optical table
6. Attach metal calibration bar to end of clamping rod where the airfoil attaches
7. Rotate the clamp until it reaches an appropriate angle (an appropriate angle is one in which the normal and axial forces are in the range of expected experimental normal and axial forces)
8. Measure the angle with an inclinometer
9. Increase the mass hanging from the hole in the metal bar 1kg at a time until the maximum expected experimental force is achieved
10. Take a reading at different AOA.
11. Plot the Inject velocity verse AOA curve.
12. Plot the lift, drag and pressure coefficient Vs. AOA curve.
13. Check to see if the airfoil is now calibrated correctly by placing known weights on the center span making sure the program is reading the correct force



APPENDIX B

LIST OF INSTRUMENTATION AND EQUIPMENT

Instrumentation Used for Wind Tunnel Experiment

Pressure Measurements:

Manometers and LAB VIEW program

Temperature Measurements:

Dry Thermometer

Flow rate control and Measurements:

Compressor, Vacuum pump, Wheel valve, gate valve, Flow meter

Equipment Used for Wind Tunnel Experiment:

ME Existing Aerolab Wind tunnel.

Computers and software Used for Wind Tunnel Experiment

Lift and Drag Measurements:

Office 2007 + Microsoft Windows 7 Professional

APPENDIX C

DETAILED AIRFOIL ASSEMBLY PROCEDURE

- 1.0 Attach L-brackets to optical table with screws and washers.
- 2.0 Attach sting clamp/cylinder assembly to injection side airfoil endplate with screws
- 3.0 Attach airfoil to injection side assembly (cylinder, clamp, endplate).
- 4.0 Attach Kiel stagnation pressure probe to suction side airfoil endplate.
- 5.0 Make sure Duocel aluminum foam is in airfoil, if not place in now
- 6.0 Attach suction side airfoil endplate to the airfoil assembly.
- 7.0 Slide the tunnel wall circular plate onto the cylinder.
- 8.0 Slide the cylinder/clamp into the collet that is attached to the optical table
- 9.0 Attach entire assembly to the wind tunnel
- 10.0 Replace Plexiglas tunnel wall with Plexiglas box tunnel wall
- 11.0 Attach internal box suction manifold to circular box wall and external box suction manifold
- 12.0 Prepare latex tubes to be attached to airfoil suction manifold
- 13.0 Attach suction manifold to the airfoil already in wind tunnel
- 14.0 Secure the Plexiglas box side of the wind tunnel
- 15.0 Place the lid on the box and screw down with screws
- 16.0 Replace ceiling and floor of wind tunnel if removed
- 17.0 Attach injection hose to hollow cylinder and secure with hose clamp
- 18.0 Attach PVC suction pipe to external manifold and wrap connection with duct tape.

APPENDIX D

DETAILED WINDTUNNEL ASSEMBLY PROCEDURE

1. Turn on vacuum pump
2. Start compressor
3. Assemble and mount airfoil as described in assembly procedure
4. Connect different probes to appropriate transducers
5. Turn on all instrumentation and computer
6. Set zero degree angle of attack
7. Rotate airfoil to desired angle of attack
8. Enter necessary information into program
 - a. Angle of attack
 - b. Ambient pressure
 - c. Ambient temperature
 - d. Area of injection jet
9. Turn on wind tunnel
 - a. Turn on wind tunnel breaker
 - b. Push forward run button on wind tunnel
 - c. Switch to Front Panel control on wind tunnel display
 - d. Rotate Fan Speed Control until desired velocity is reached
10. Start air injection
 - a. Make sure that control wheel valve is open
 - b. connection of compressor pipe with control valve is correct
 - c. Slightly adjust the valve upstream of the control valve to fine tune the mass flow rate
11. Dial in suction mass flow rate
12. Only continue after the suction mass flow rate is desirable
13. Start air suction and sampling.